Optical backscattering by particles in Arctic seawater and relationships to particle mass concentration, size distribution, and bulk composition

Rick A. Reynolds,* Dariusz Stramski, Griet Neukermans[†]
Marine Physical Laboratory, Scripps Institution of Oceanography, University of California San Diego, La Jolla, California 92093-0238, USA

Abstract

The magnitude and spectral shape of the optical backscattering coefficient of particles, $b_{bp}(\lambda)$, is being increasingly used to infer information about the particles present in seawater. Relationships between b_{bp} and particle properties in the Arctic are poorly documented, and may differ from other oceanic regions which contribute the majority of data used to develop and parameterize optical models. We utilize recent field measurements from the Chukchi and Beaufort Seas to examine relationships between the spectral backscattering coefficient of particles in seawater and the mass concentration, bulk composition, and size distribution of the suspended particle assemblage. The particle backscattering coefficient spanned six orders of magnitude from the relatively clear waters of the Beaufort Sea to extremely turbid waters on the Mackenzie shelf. This coefficient was highly correlated with the mass concentration of particles, and to a lesser extent with other measures of concentration such as particulate organic carbon or chlorophyll *a*. Increased backscattering and high mass-specific $b_{bp}(\lambda)$ was associated with mineral-rich assemblages that tended to exhibit steeper size distributions, while reduced backscattering was associated with organic-dominated assemblages having a greater contribution of large particles. Our results suggest that algorithms which employ composition-specific relationships can lead to improved estimates of particle mass concentration from backscattering measurements. In contrast to theoretical models, however, we observe no clear relationship between the spectral slope of $b_{bp}(\lambda)$ and the slope of the particle size distribution in this environment.

The inherent optical properties (IOPs) of seawater, including the spectral absorption coefficient and the volume scattering function describing the intensity and angular distribution of scattered light, largely determine the propagation of light through the ocean. The IOPs are directly linked to the concentrations and types of optically-significant constituents of seawater, many of which are of ecological and biogeochemical interest. Suspended particles comprise one such constituent that is ubiquitous in the marine environment and contributes substantially to observed variability in the absorption and scattering properties of seawater.

*Correspondence: rreynolds@ucsd.edu

[†]Present address: Takuvik Joint International Laboratory, Université Laval, Québec, Canada

The spectral backscattering coefficient, denoted $b_b(\lambda)$ where λ represents the wavelength of light in vacuo, describes the amount of light scattered backwards with regards to the direction of light propagation. Specifically, it is derived from the volume scattering function, $\beta(\psi,\lambda)$, through integration over the backward hemisphere

$$b_b(\lambda) = 2\pi \int_{\pi/2}^{\pi} \beta(\psi, \lambda) \, \sin\psi \, d\psi \tag{1}$$

where ψ is the scattering angle. Within aquatic environments, the contribution by dissolved organic materials and turbulence to $b_b(\lambda)$ is generally negligible and the total backscattering coefficient can be considered as the sum of the contributions to backscattering by water molecules, $b_{bw}(\lambda)$, and particles, $b_{bp}(\lambda)$. We note that the particle fraction includes the scattering contribution of very small particles (e.g., colloids) which pass through typical membrane or glass-fiber filters, and thus are often operationally included in the dissolved fraction (Stramski and Woźniak 2005; Zhang and Gray 2015). As the scattering properties of water
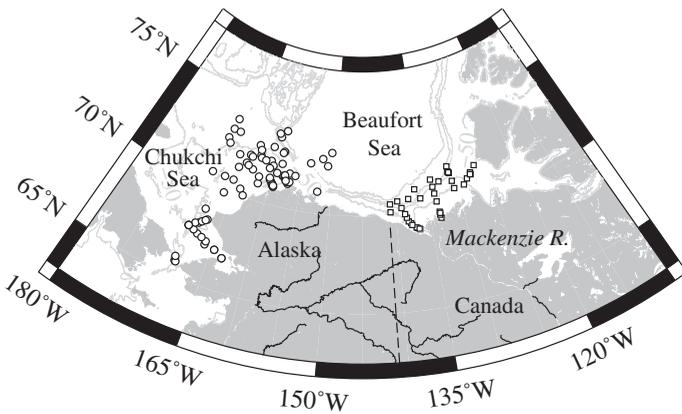
Fig. 1. Map of study area depicting sampling locations for the MALINA (square symbols) and the ICESCAPE (circles) cruises.

molecules vary within a narrow range, the variability in backscattering by seawater is driven primarily by changes in $b_{bp}(\lambda)$.

Sensors for measuring optical backscattering are commercially available and increasingly deployed on in situ sampling platforms such as ships, moorings, and autonomous underwater vehicles (e.g., Boss and Behrenfeld 2010; Antoine et al. 2011; Briggs et al. 2011). Furthermore, the backscattering coefficient is directly linked to ocean reflectance and can be estimated from measurements of ocean color obtained from air- or spaceborne sensors (Loisel and Stramski 2000; Lee et al. 2002; Maritorena et al. 2002), extending observations of surface waters to large spatial and temporal scales. As a result, there is strong interest in using b_{bp} as a means to infer information on the suspended particle assemblage of seawater. The magnitude of b_{bp} has been utilized in the development of algorithms to estimate concentrations of suspended particle mass (Downing 2006; Boss et al. 2009), particulate organic carbon (POC) (Stramski et al. 1999, 2008), phytoplankton carbon (Behrenfeld et al. 2005; Martinez-Vicente et al. 2013), and phytoplankton growth rates (Behrenfeld et al. 2005). The spectral shape of $b_{bp}(\lambda)$ has also been proposed as an indicator of the particle size distribution (PSD) (Loisel et al. 2006; Kostadinov et al. 2009) and to characterize phytoplankton community structure (Kostadinov et al. 2010; Fujiwara et al. 2011).

Variability in the particle backscattering coefficient can arise from changes in particle concentration, refractive index (related to composition), size, and shape. Most understanding of the interaction between backscattering and these particle characteristics have come from modeling studies which utilize idealized particle assemblages coupled with theoretical descriptions of particle absorption and scattering (e.g., Stramski and Kiefer 1991; Stramski et al. 2004). This approach provides useful insights into the general trends describing backscattering by various types of particles, but

has inherent limitations for predicting complex natural seawater assemblages. Similarly, although there are an increasing number of in situ measurements of backscattering from aquatic environments with natural particle assemblages, it is rare that these studies also incorporate complementary measurements of the characteristics of the particles present in the assemblage, limiting the interpretation of observed patterns.

The Arctic Ocean is a region experiencing rapid environmental change. Because of this region's remoteness and inaccessibility throughout much of the year, the use of remotely-sensed optical measurements represents an important tool for monitoring spatial and temporal changes in this ecosystem. A major challenge for these applications is that Arctic waters are strongly influenced by extensive shelves and river input from surrounding landmasses, resulting in much higher optical complexity than in lower latitude open oceans which provide the bulk of data for parametrization of bio-optical relationships and empirical algorithms. Several studies over the past decades have suggested that relationships between chlorophyll *a* concentration (Chl*a*), absorption, and ocean color in the Arctic vary markedly from lower latitudes, and that the application of global algorithms can result in large errors in predictions of Chl*a* and other seawater constituents (Mitchell 1992; Cota et al. 2003; IOCCG 2015).

There are reasons to hypothesize that scattering properties of suspended particle assemblages in the Arctic may also differ considerably from lower latitude open oceans. Large riverine inputs and resuspension on shallow coastal shelves suggest an important potential contribution of inorganic particles to optical properties in many regions. Sediment particles can also be transported by ice and released during melting (Darby et al. 2011). The presence of large, heavily-pigmented phytoplankton cells acclimated to low irradiance and a prevalence of species forming colonies or chains can also lead to unique scattering properties.

In this study, we describe measurements of spectral backscattering from both coastal and offshore locations in the Arctic Ocean, including measurements made in regions within sea ice cover. In situ measurements of the spectral backscattering coefficient were obtained in conjunction with water sample analyses to characterize the bulk composition and size distribution of suspended particles. Using this information, we examine variation in the magnitude and spectral shape of the particulate backscattering coefficient and its relationships to characteristics of the particle assemblage.

Materials and methods

Study area

Measurements were obtained on three expeditions to the western Arctic Ocean (Fig. 1). The MALINA (MAckenzie LIght aNd cArbon) cruise occurred in the southeastern Beaufort Sea during the period from 31 July to 24 August 2009

on the *CCGS Amundsen* (e.g., Matsuoka et al. 2012). The station grid bracketed the outflows of the Mackenzie River, with transects extending from the delta to the southernmost limit of the pack ice outside the continental shelf. Two cruises associated with the NASA ICESCAPE (Impacts of Climate on EcoSystems and Chemistry of the Arctic Pacific Environment) program utilized the *USCGC Healy* to sample the Chukchi Sea and western Beaufort Sea during two successive years; from 18 June through 16 July 2010 and from 28 June through 24 July 2011 (Arrigo 2015). Sampling on these cruises included transects where measurements were done from open water across the ice edge to several kilometers within consolidated pack ice. For the three cruises, 121 stations which included measurements of backscattering were completed.

The instrumentation and methodology used for the collection and processing of data were nearly identical among all three cruises, with only minor exceptions as noted in the following sections.

Bulk measures of particle mass concentration and composition

Immediately before or after in situ optical measurements, water samples were collected at discrete depths from a CTD-Rosette equipped with Niskin bottles. The depths chosen for analysis always included near surface water ($\sim$ 1–3 m nominal depth), and additional depths associated with features such as the chlorophyll *a* fluorescence maximum, maxima in optical beam attenuation or backscattering, or within 3–5 m of the bottom for regions on the shelf. For stations located off the shelf with water depths exceeding 2000 m, samples at 300 m were taken to provide reference measurements of optically clear waters. Samples obtained from each depth were collected by opening the bottom closure of each Niskin bottle and draining the entire bottle into 20 L carboys to ensure collection of all particles. Subsamples for each analysis were subsequently withdrawn from the carboy after mixing to ensure homogeneity among measurements. Filtration volumes for each measurement were adjusted based on observed particle concentration and optimized for each individual analysis, with values ranging from 30 mL to 11 L.

Concentrations of particle dry mass, organic carbon, and phytoplankton pigments were used to characterize the bulk particle assemblage. The mass concentration of dried suspended particulate matter per unit volume of water, SPM, was determined gravimetrically after filtration under low vacuum onto pre-rinsed, pre-combusted glass-fiber GF/F filters (25 mm diameter) that were weighed prior to use. Following filtration, sample filters and edges were rinsed with deionized water to remove residual sea salt, dried at 60°C, and stored sealed until analysis. The mass of particles collected on the filters was measured with a Mettler-Toledo MT5 microbalance with 1 μg precision. Typically 2 to 3 replicate filters were measured for each sample, with a median

precision of 11% observed for MALINA ($n = 124$) and 3% for ICESCAPE ($n = 81$).

The concentration of particulate organic carbon, POC, was obtained using a method consistent with established protocols (e.g., Knap et al. 1996). Water samples were filtered through precombusted 25 mm GF/F filters, and filters were transferred to clean glass scintillation vials, dried at 60°C, and stored until post cruise analysis. Organic carbon content of each filter following acidification to remove inorganic carbon was determined with standard CHN analysis involving high temperature combustion of sample filters (Parsons et al. 1984). For MALINA, POC was measured from combustion of the same filters used in SPM determination. A number of unused filters from each lot of precombusted filters were used to quantify the background carbon content of filters and subtracted from the sample data. Sample filtration volumes were large enough to ensure that contributions of the blank filter (7 ± 2.1 μg C, mean $\pm$ standard deviation) and typical values of adsorbed dissolved organic carbon ($\sim$ 11 μg C per filter, Cetinić et al. 2012) were small relative to the measured carbon content of the sample filter (319 ± 195 μg C). Duplicate or triplicate samples for POC were taken for each station and averaged to produce the final result of POC. The median coefficient of variation for replicate samples was similar to that observed for SPM; 11% for MALINA ($n = 123$) and 3% for ICESCAPE ($n = 82$).

Samples for phytoplankton pigments were filtered on 25 mm GF/F filters under low light and flash frozen in liquid nitrogen until analysis by High Performance Liquid Chromatography (HPLC). MALINA samples were analyzed using the analytical procedure described in Ras et al. (2008), and ICESCAPE samples were determined using the method of Van Heukelem and Thomas (2001). In this study we use the HPLC-determined concentration of total chlorophyll *a* as the measure of Chl*a*, which represents the summed concentrations of mono- and divinyl chlorophyll *a*, chlorophyllide *a*, and the allomeric and epimeric forms of chlorophyll *a*.

Particle size distribution

Two independent methods utilizing different principles were employed to estimate the PSD. At each station, a Laser In Situ Scattering and Transmissometry instrument (LISST-100X type B, Sequoia Scientific) was deployed on a vertical profiling instrument package. The LISST provides in situ measurements of forward light scattering from a laser beam ($\lambda = 532$ nm) in 32 scattering angles over the approximate angular range $\psi = 0.08$–13.5° (Agrawal and Pottsmith 2000). The space surrounding the optical path was baffled to avoid effects of ambient light on LISST measurements (Reynolds et al. 2010; Andrews et al. 2011). The concentration of particle volume within a size bin with median particle diameter D, $V(D)$, was obtained for 32 particle size bins through inversion of the scattering pattern utilizing an inversion kernel matrix derived from scattering patterns of spherical

homogenous particles computed from Mie theory for a real-istic range of index of refraction. The resulting volume distri-butions cover the approximate size range of 1–200 μm. Because the inversion exhibits stronger dependence on refractive index for the smallest particles (Andrews et al. 2010) and may also be sensitive to particle shape effects in this size range (Agrawal et al. 2008), measurements from the first seven size bins ($D < 3.2$ μm) were excluded from further analysis as in Reynolds et al. (2010). As a result, the LISST-derived $V(D)$ reported here consists of 25 size bins spanning the size range 3.2–198.6 μm. The concentration of particle number within each size bin, $N(D)$, was computed from the $V(D)$ by assuming spherical particles.

In addition to the LISST measurements, the PSD of water samples collected with the CTD-Rosette was measured with a Beckman-Coulter Multisizer III using 0.2 μm filtered seawater as the blank. Samples were routinely measured with a combi-nation of two aperture sizes (30 μm and 200 μm), which when combined span the particle diameter range of 0.7–120 μm. Both apertures were calibrated using solutions contain-ing NIST-traceable microsphere standards of known size.

Each discrete Coulter measurement consisted of a set of values representing the number of particles per unit volume within a size class, $N(D)$. Size classes consisted of 256 bins logarithmically spaced over the measured range, ensuring a very high size resolution of measurements. The width of individual size bins is dependent upon the aperture size and diameter of the size class; for example, ΔD ranges from as lit-tle as 0.01 μm for the 30 μm aperture to as large as 1.6 μm for the 200 μm aperture.

Multiple (>25) replicate measurements of the PSD were taken with the Coulter for each sample and summed to pro-vide larger sample volumes and improved statistical accu-racy. Total sample volumes after this summation averaged about 100 μL for the 30 μm aperture and 165 mL for the 200 μm aperture. The density function of the differential particle number distribution, $F_N(D)$, was calculated by normalizing the concentration of particles within each size bin to the bin width. To create the final distribution, measurements from both apertures were merged at an overlapping size class ($D \sim$ 4.8 μm) which shared a similar midpoint and bin width.

The use of two independent methods for obtaining the PSD is advantageous as there is no single existing technique which provides high resolution, accurate measurement of the PSD over the entire optically or biogeochemically-relevant size range of aquatic particles. The LISST and Coulter techniques each have inherent advantages and dis-advantages. The LISST is based on an optical scattering mea-surement capable of rapid (1 Hz) sampling, and thus can provide in situ measurements which are collected contempo-raneously with other optical measurements. However, the inversion of the bulk scattering signal from an assemblage of particles requires assumptions concerning particle properties which may not be well satisfied in natural assemblages of diverse aquatic particles, and provides relatively course reso-lution over the size range 3–200 μm. In contrast, electrical impedance methods such as the Coulter technique are easily calibrated with known standards, and yield high-resolution measurements of size on individual particles. As a benchtop measurement, however, the requirement to work with dis-crete samples removed from the environment can lead to potential modification of the particle assemblage during sampling or during the measurement process. The method is also laborious and time consuming because of the need to sample sufficient volumes of seawater to yield statistical accuracy, and thus the analysis is limited to a small number of discrete samples at a given station.

Because of the advantages and limitations associated with each technique, in this study we show results obtained from both methods. Apart from differences in the principal assumptions underlying the two measurements, each instru-ment has a different particle size range, resolution of particle size, and interrogated volume of sample. Quantities derived from the resulting PSDs are therefore not strictly equivalent, but are shown to provide general confirmation of observed trends in the data.

Various metrics computed from the measured size distri-butions obtained from both the LISST and Coulter counter were used to characterize samples. The density function of particle number concentration was fitted to a power law model (Bader 1970; Jonasz and Fournier 2007)

$$F_N(D) = N_o \left(\frac{D}{D_o}\right)^{\zeta} \tag{2}$$

where D_o is a reference diameter, N_o is the value of the func-tion at D_o, and ζ is the dimensionless slope of the distribu-tion. The proportion of particle projected area contributed by particles exceeding 20 μm in diameter, A_L, was computed from the particle area distribution as an indicator of the rela-tive importance of large particles (e.g., microplankton size range). For the Coulter measurement, these metrics were computed over the size range 0.7–100 μm, and for the LISST a size range of 3.2–198.6 μm was utilized.

Backscattering measurements

At each station, an instrument package containing a suite of sensors was deployed to obtain vertical profiles of in situ optical properties. The spectral backscattering coefficient, $b_b(\lambda)$, was determined with a combination of Hydroscat-6 and a-βeta sensors (HOBI Labs, Inc.). These instruments, cali-brated by the manufacturer immediately before or after each cruise, provide a measurement of the spectral volume scat-tering function $\beta(\psi)$ at an effective scattering angle $\psi = 140°$ (Maffione and Dana 1997). For MALINA, a single multispec-tral Hydroscat-6 was paired with two single wavelength a-βetas to yield measurements in eight spectral bands (nomi-nal center wavelengths of 420, 442, 470, 510, 550, 589, 620,
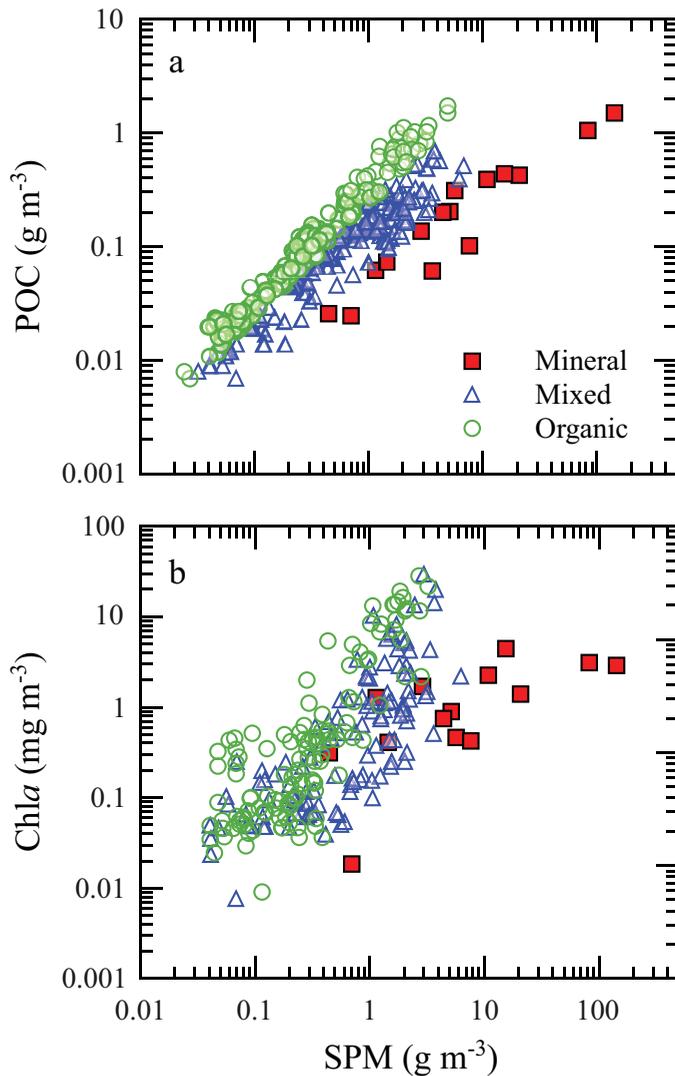
Fig. 2. Scatter plots illustrating the relationship between suspended particle dry mass concentration, SPM, and **(a)** concentration of particulate organic carbon, POC, and **(b)** concentration of chlorophyll *a*, Chl*a*. In each panel, the predominant particle composition as defined by the POC/SPM ratio is indicated.

and 671 nm). For both ICESCAPE cruises, two Hydroscat-6 instruments with complementary wavelength sets were deployed to provide estimates in eleven spectral bands spanning the UV/VIS/NIR spectral region (394, 420, 442, 470, 510, 532, 550, 589, 649, 730, and 852 nm). One wavelength (550 nm) was common to both instruments for the purpose of intercomparison. The comparison at this band for the two instruments yielded a median ratio of 0.99, with a linear slope of 0.96 (± 0.02) and an intercept statistically indistinguishable from zero. The 420-nm band on the MALINA cruise and the 442-nm band on the 2010 ICESCAPE cruise failed to operate correctly, and these data were excluded from subsequent analyses.

The values of $b_b(\lambda)$ were calculated based on a method described originally by Maffione and Dana (1997), and a detailed description of the procedure is provided in Stramski et al. (2008). Briefly, the spectral backscattering coefficient was obtained from the measured $\beta(140°,\lambda)$ using the relation

$$b_b(\lambda) = b_{bp}(\lambda) + b_{bw}(\lambda) = 2\pi\chi[\beta(140°,\lambda) - \beta_w(140°,\lambda)] + b_{bw}(\lambda) \quad (3)$$

where the subscripts p and w indicate, respectively, the contributions from particles and pure seawater to total scattering. Pure water values for $\beta_w(140°,\lambda)$ and $b_{bw}(\lambda)$ were calculated by using measured water temperatures as input to the equations of Buiteveld et al. (1994), but a depolarization ratio of 0.039 for water molecules was chosen based on the review of Jonasz and Fournier (2007). Calculated pure water values were subsequently adjusted for seawater using measured salinity S and a multiplicative adjustment factor of $[1 + 0.3S/37]$ (Morel 1974; Twardowski et al. 2008). A spectrally constant value of 1.13 was assumed for the parameter χ representing the relationship between $\beta_p(140°,\lambda)$ and $b_{bp}(\lambda)$ (Dana and Maffione 2002).

For each spectral band, backscattering measurements were corrected for the attenuation of light along the optical path length using the so-called σ-correction (Maffione and Dana 1997). This correction utilizes the parameter $K_{bb}(\lambda)$ estimated from the relation $K_{bb}(\lambda) = a_p(\lambda) + a_g(\lambda) + 0.4b_p(\lambda)$ (HOBI Labs Hydroscat-6 manual Rev. J, 2010), and was parameterized based on independent determinations of the spectral absorption coefficient by particles, $a_p(\lambda)$, the spectral absorption coefficient of colored dissolved organic material, $a_g(\lambda)$, and the spectral scattering coefficient by particles, $b_p(\lambda)$ (Neukermans et al. 2014). At a wavelength of 420 nm, the median value of the correction factor for this dataset is 4%, with the correction exceeding 25% in 5% of the data. Values of the correction are smaller with increasing wavelength. For the few samples representing the very turbid waters of the Mackenzie River plume, the calculated correction is extremely large (> fivefold) and the validity of this correction is questionable. These data were not utilized in subsequent analyses.

Vertical profile data of $b_b(\lambda)$ were filtered to remove spikes and averaged into 0.5 m or 1 m depth bins for analysis and correlation with discrete water samples.

Regression analyses

General correlations between particle characteristics and optical coefficients investigated in this study utilize Model II regression analysis, which is appropriate when measurement uncertainties are present in both measured variables. These regression results were calculated using the geometric mean (reduced major axis) model following Ricker (1973). Standard Model I regression analysis was used to determine relationships for predicting particle mass concentration (e.g.,
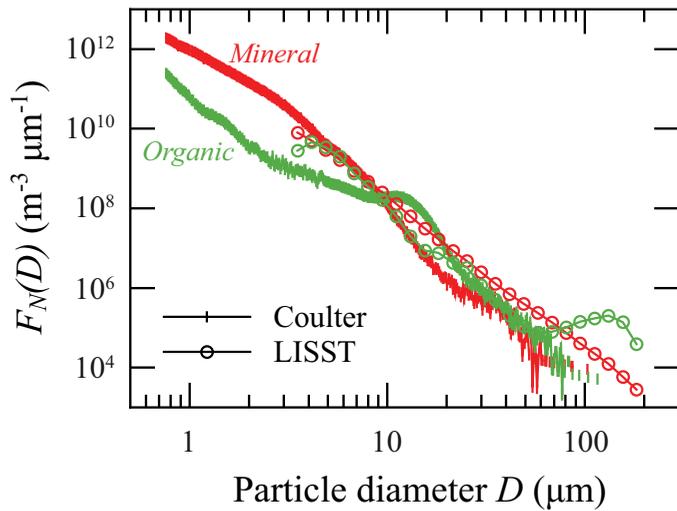
Fig. 3. Example density functions of particle number concentration, $F_N(D)$, determined for an organic-dominated (green color) and a mineral-dominated (red color) sample from the ICESCAPE 2011 cruise. For each sample, determinations were made both in vitro with a Coulter counter and in situ with a LISST-100X.

SPM, POC) from the measured particle backscattering coefficient. For relationships which assume a power function of the form $Y = k_1 [X]^{k_2}$, the $\log_{10}$ transform of the data was used as input to the regression model.

Results

Particle mass concentrations

The dry mass concentration of particles varied more than three orders of magnitude throughout the study region. Values of SPM less than 0.05 g m^{-3} were observed in offshore waters of the Beaufort Sea, but exceeded 50 g m^{-3} in shallow waters near the outflow of the Mackenzie River. Variations in SPM were accompanied by changes in other measures of particle mass concentration, including both POC and Chl*a* (Fig. 2). POC exhibits the highest degree of correlation with SPM ($r > 0.88$, $p < 0.01$), with Chl*a* exhibiting a weaker but still significant relationship.

Following the approach of Woźniak et al. (2010), we partition our dataset into three broad compositional classes based on the contribution of organic carbon to total particle mass concentration in the sample; mineral-dominated (POC $\leq 6\%$ of SPM), organic-dominated (POC $\geq 25\%$), and "mixed" assemblages of intermediate contribution (POC between 6% and 25%). In Fig. 2, different symbols are used to delineate the three assemblages based on this criterion. These categories represent arbitrary divisions along a continuum of particle mixtures, but provide a useful means of initially classifying particle assemblages and interpreting associated optical measurements.
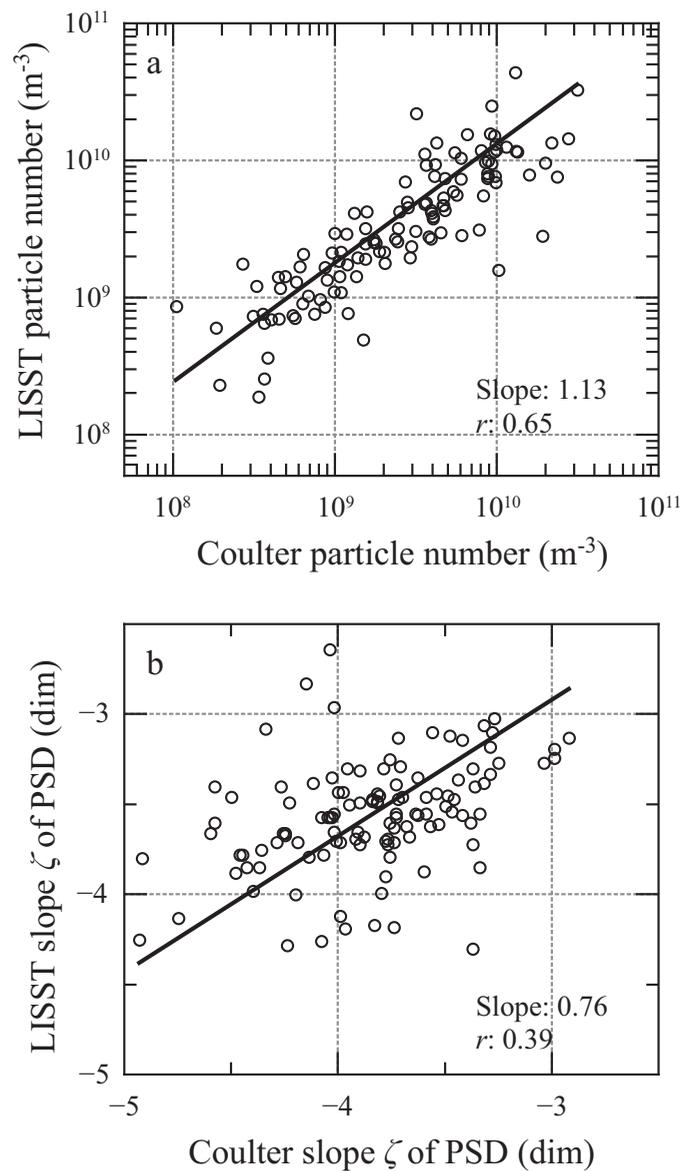

Fig. 4. Comparison of metrics from the particle size distribution determined from the Coulter counter and LISST on coincident samples. Metrics were computed for the size range of 3.2–100 μm from both instruments. Solid lines represent the fit of a Model II regression, with the slope and correlation coefficient r indicated. **(a)** Integrated particle number concentration. **(b)** The slope parameter ζ of the particle number distribution.

Particle size distributions

Example size distributions measured by both the Coulter and LISST are illustrated in Fig. 3. Two samples are depicted, both from a transect along the Chukchi Sea shelf during the 2011 ICESCAPE cruise. The mineral-dominated assemblage was collected a few meters above the seafloor, while the organic sample was from 25 m depth within a layer corresponding to an under-ice phytoplankton bloom dominated by the presence of large planktonic diatoms (Arrigo et al.
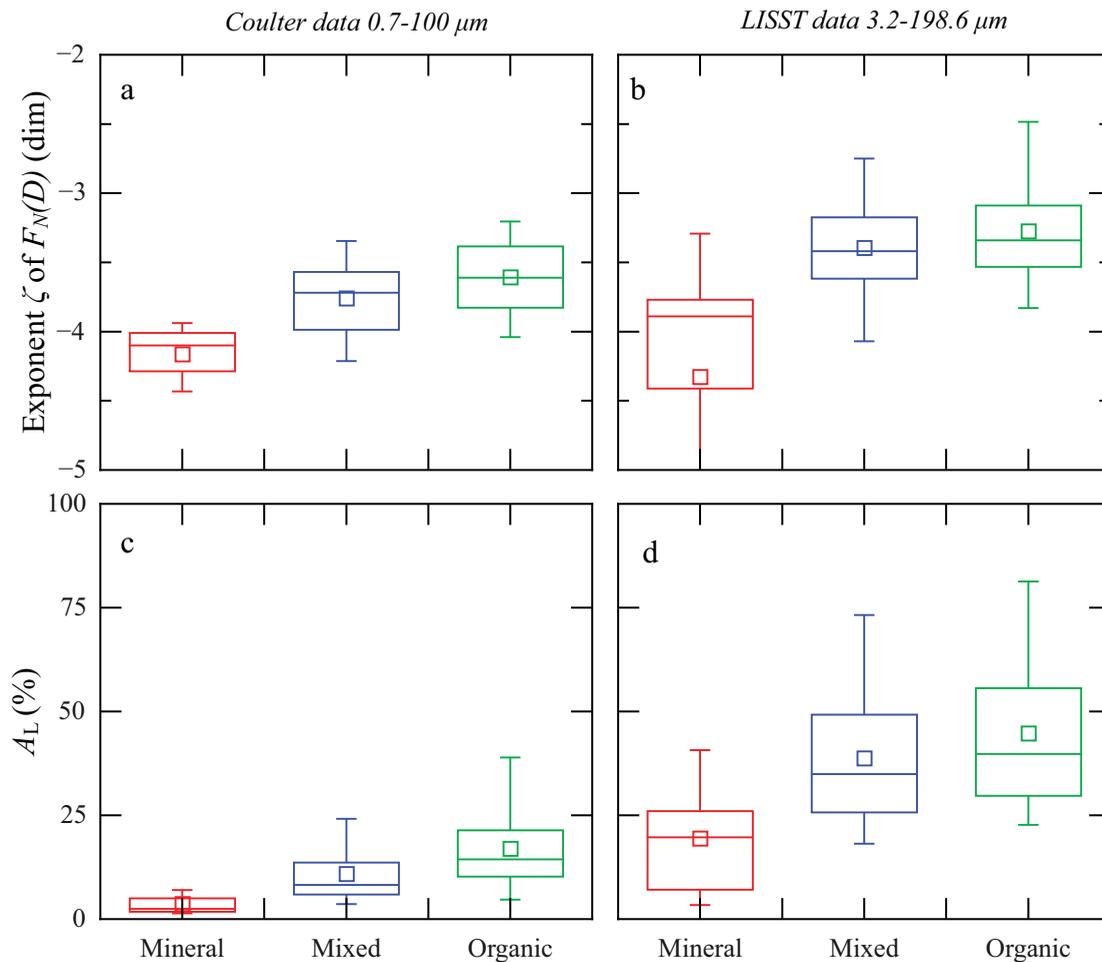
Fig. 5. Boxplots illustrating the range of values associated with characteristics of the particle size distribution determined from measurements with either the Coulter counter (panels a and c, size range 0.7–100 μm) or the LISST (panels b and d, 3.2–198.6 μm) for each particle compositional type. Top panels depict the power law slope of the PSD over the indicated size range, and the bottom panels depict the percentage of projected-area represented by particle diameters greater than 20 μm. In these plots, the mean is indicated by the small square, the median by the horizontal line, the box represents the 25th–75th percentile range, and the whiskers denote the 5th and 95th percentiles.

2014). For the mineral-dominated assemblage, the number distribution is generally featureless, has a steeper overall slope across the distribution, and particles of diameters less than 10 μm have a greater contribution to the assemblage. In contrast, the organic assemblage size distribution exhibits a flatter but more variable slope with the presence of significant peaks corresponding to increased concentrations of particles within specific size ranges. Both size distributions show changes in slope across the size range, highlighting the difficulty in characterizing the distributions with a model consisting of a single slope value. The observed differences in shape of the PSD suggest strong potential differences in the optical properties of these two assemblages.

Figure 3 also provides a comparison of the distributions determined from the in vitro Coulter measurement with the in situ LISST measurement. For the majority of samples, the agreement between the two measurements is reasonable

with the largest differences generally observed in the larger size ranges ($D > 50$ μm) where Coulter counts have higher statistical uncertainties and the presence of phytoplankton colonies or particle aggregates may be important. The two distributions depicted in Fig. 3 were chosen to illustrate trends in the PSD based on composition, and although both techniques are generally comparable in magnitude and capture the general trends associated with each sample, some important differences can be observed. For the mineral-dominated assemblage, the Coulter and LISST agree well for particle diameters less than 10 μm, but the Coulter data exhibit a more rapid decline in concentration for larger particles than observed with the LISST. Consequently, the computed slope of the PSD over the entire distribution from the Coulter ($\zeta = -4.9$) is much steeper than that determined by the LISST ($\zeta = -3.8$). For the organic assemblage, both instruments yield a flatter overall slope but show the presence of
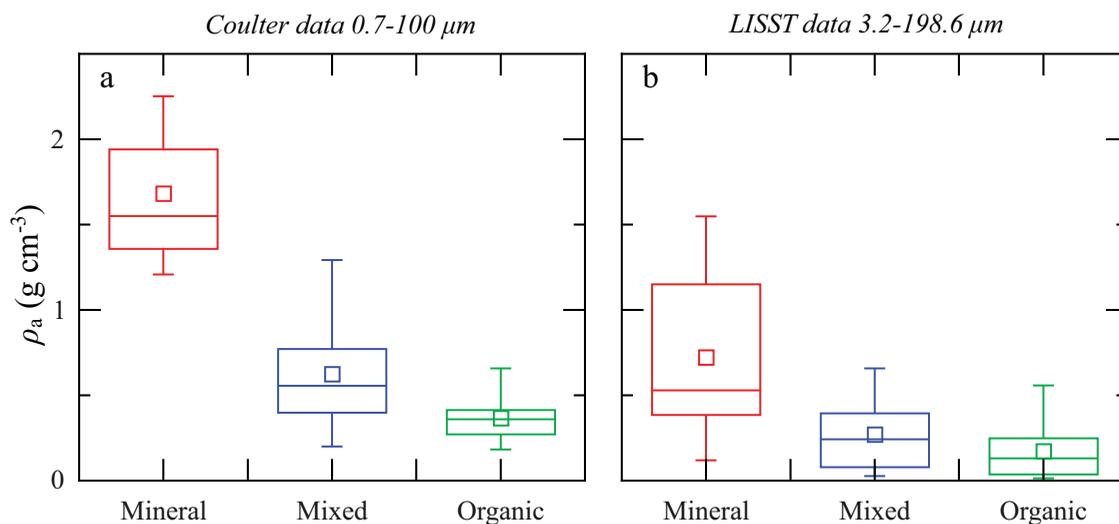
Fig. 6. Boxplots illustrating the range of values for the apparent mean particle density (ρ_a) determined from measurements with either the Coulter counter **(a)** or the LISST **(b)** for each particle compositional type. Particle density was calculated as the ratio of SPM to total particle volume concentration integrated over the size range indicated.

prominent peaks at various size ranges throughout the distribution.

To compare characteristics of the PSD provided by both instruments, we computed metrics of the PSD for 118 samples where contemporaneous measurements were available (Fig. 4). A size range common to both instruments, 3.2–100 μm, was used for this comparison. The upper limit of 100 μm for the Coulter was chosen to avoid regions of low particle counts and high statistical noise at larger particle diameters. For the LISST, the upper limit of the closest corresponding size bin is 103 μm. The total number of particles, N_t, integrated over this size range was well-correlated between the instruments with a slope of 1.13. A reasonable correlation, albeit with considerable scatter, was also observed in the estimated slope ζ of $F_N(D)$. For the size range 3.2–100 μm, the slopes calculated from the LISST measurement tend to be flatter (less negative) than those obtained from the Coulter, on average by about ~7%.

The differences in the PSDs observed in Fig. 3 are consistent with overall trends of the data, in which a general covariation was observed between the dominant particle composition and the relative abundance of small and large particles (Fig. 5). For both Coulter and LISST measurements (Fig. 5a,b), the average value of the slope ζ describing the number distribution is significantly different among the three compositional classes (single-classification ANOVA, $p < 0.001$). Mineral-dominated assemblages generally exhibit the steepest overall slope of $F_N(D)$, with 75% of the measurements with slopes steeper than a value of -3.7 in the case of the LISST measurements. The flattest (less negative) values of slope are associated with the organic-dominated assemblages (-3.3 ± 0.4, LISST), with intermediate values for the assemblages of mixed composition. Similarly, the proportion of par-

ticle projected area contained within large diameter (> 20 μm) particles varies with composition (Fig. 5c,d). For mineral assemblages, on average only 20% of the total area within the LISST measured size range is contained within particles greater than 20 μm. This contrasts strongly with organic assemblages, where particles greater than 20 μm have a nearly equal contribution (45%) to that of smaller particles. Similar qualitative trends are observed in the Coulter data.

Apparent particle density

The observed trends in size distribution imply differences in the average particle density among the three compositional classes. The particle density is a measure of the relative amounts of water and solid material within a particle, and this physical property can be considered an indicator of the bulk particle refractive index which in turn strongly influences optical behavior. For each sample with concurrent measurements of particle mass concentration and PSD, we computed the mean apparent density of particles, ρ_a, as the ratio of SPM/V_t, where V_t is the total particle volume integrated over the measured size range per unit volume of seawater. As noted previously, this size range differs between the Coulter (0.7–100 μm) and the LISST (3.2–198.6 μm) and thus the computed values differ between the instruments. It is also important to note that the measurement of SPM is derived from filtration on GF/F filters with nominal pore size of ~ 0.7 μm, thus the computed values of ρ_a using Coulter measurements begin at a comparable size range. In contrast, values of ρ_a estimated from the LISST omit the size range < 3.2 μm and thus likely overestimate the true value, and the extent of this error will depend on the PSD (Bowers et al. 2009).

All assemblages exhibit a wide range of ρ_a values, with the lowest variability observed for mineral-dominated assemblages
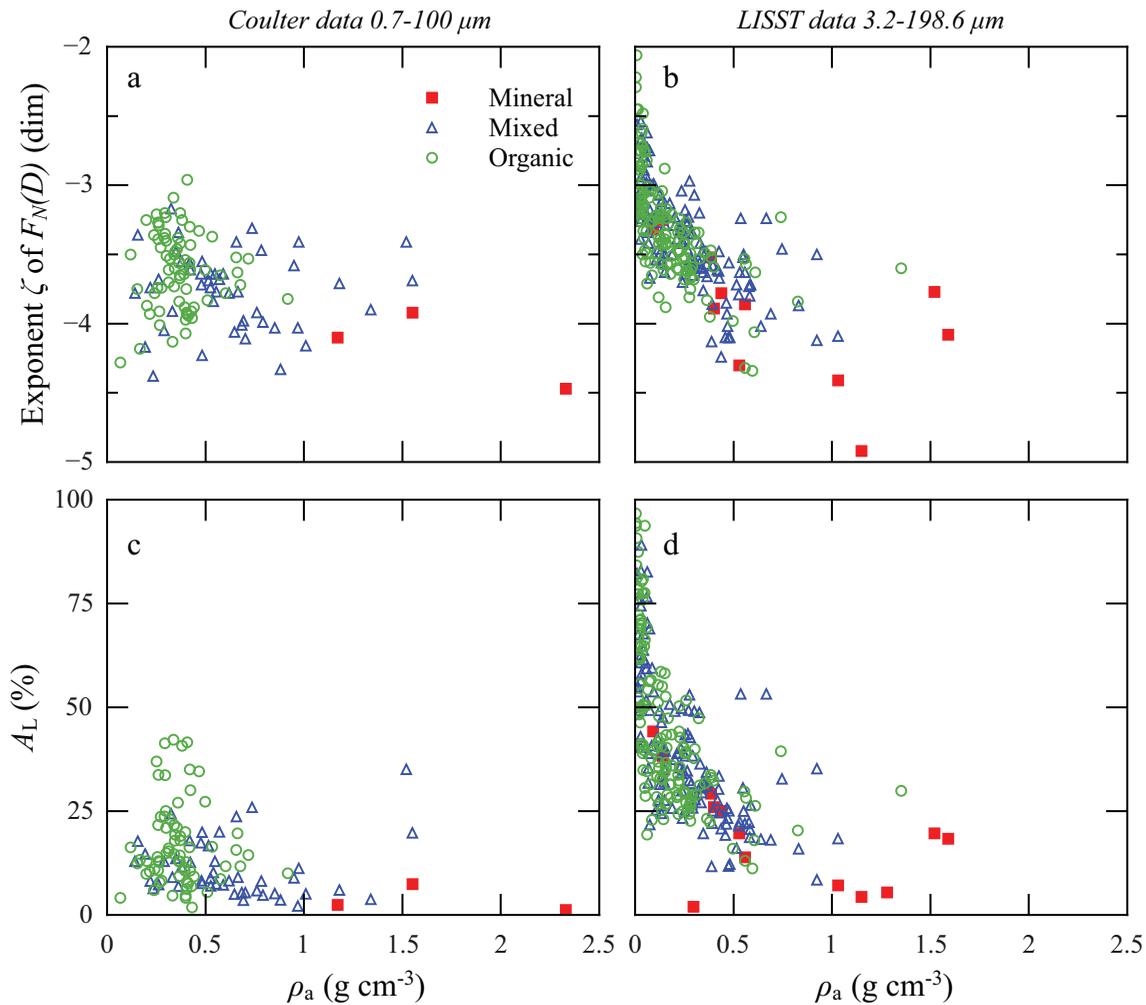
Fig. 7. Relationships between the power law slope of the PSD and apparent mean particle density for data calculated using the Coulter counter **(a)** or LISST **(b)** measurements. **(c, d)** Similar to panels a and b, but for the percentage of projected-area represented by particle diameters greater than 20 μm.

(Fig. 6). Values obtained with the Coulter, in which V_t is determined over a narrower size range, are naturally higher than those calculated with LISST but both exhibit similar trends. Mineral assemblages have the highest average values, with three values computed from the Coulter data for this assemblage ranging from 1.17 g cm^{-3} to 2.33 g cm^{-3}. For the more numerous LISST data ($n = 13$), the mean value is 0.7 g cm^{-3} with a highest value of 1.6 g cm^{-3}. These values approach or are within the range of 2–5 g cm^{-3} reported for suspensions of pure minerals or solid non-aggregated mineral particles in coastal waters (Berry and Mason 1959; Lide 2001; Woźniak and Stramski 2004). The mean values of ρ_a for organic-dominated assemblages determined from both Coulter (0.37 g cm^{-3}) and LISST (0.17 g cm^{-3}) are less than 25% of the average mineral-dominated value, and these values are within the range of measurements that have been reported for pure cultures of phytoplankton (0.17–0.85 g cm^{-3}; Aas 1996).

The results depicted in Figs. 5, 6 suggest a degree of covariation between particle density and indicators of particle size. For both instruments, similar tendencies were observed between mean particle density and two descriptors of the PSD, the number distribution slope ζ (Fig. 7a,b) and the percentage of particle area represented by particles greater than 20 μm (Fig. 7c,d). The higher values of density, typically associated with mineral assemblages, exhibit steeper declines in particle number with increasing diameter and a corresponding reduction in the contribution of larger particles to particle projected area. In contrast, flatter slopes of the PSD containing a greater contribution of large particles are mostly associated with organic-dominated assemblages of low mean particle density (low refractive index). The observed trends in both refractive index and size distributions can lead to optical differentiation between the three types of assemblages (e.g., Babin et al. 2003).

Particle backscattering coefficient

Measured values of $b_{bp}(\lambda)$ vary six orders of magnitude in the combined dataset, generally decreasing with increasing wavelength for any given spectrum (Fig. 8a). A similar range

of values is observed in the MALINA and ICESCAPE cruises for the majority of measurements, but the highest values were all obtained during MALINA. The clearest waters are associated with stations sampled outside the continental shelf within the Beaufort Sea. In these locations, the magnitude of $b_{bp}(\lambda)$ was less than 0.005 m^{-1} in the visible spectral region and molecular scattering by water contributed as much as 70% of the total backscattering coefficient in the blue spectral region. The largest values of $b_{bp}(\lambda)$, exceeding 0.1 m^{-1}, were observed at turbid nearshore stations located within the plume of the Mackenzie River.

To examine the wavelength dependency of particle backscattering, discrete spectral measurements were fit to a power function of the form

$$b_{bp}(\lambda) = b_{bp}(\lambda_o)\left(\frac{\lambda}{\lambda_o}\right)^{\eta} \tag{4}$$

where λ_o represents a reference wavelength and η is the dimensionless spectral slope of $b_{bp}(\lambda)$. Because the 442 nm spectral channel failed to operate for the ICESCAPE 2010 cruise, this wavelength was also excluded when fitting spectral relationships from ICESCAPE 2011 to ensure consistency between cruises. This band is located within a principal absorption maximum associated with chlorophyll *a* and other major phytoplankton accessory pigments, and thus also potentially subject to effects of so-called anomalous dispersion in the presence of strong absorption features (van de Hulst 1957; Morel and Bricaud 1981). Figure 8b illustrates example measurements of $b_{bp}(\lambda)$ for two samples of differing turbidity from the ICESCAPE 2011 cruise, and includes the fit of Eq. 4 obtained by least squares linear regression on the log$_{10}$-transformed data.

For the majority of observations, Eq. 4 provides a good description of the measured data over the entire spectral range from 394 nm to 852 nm. Residual differences between measured values (b_{bp}^{obs}) and the values obtained from the fitted model (b_{bp}^{fit}) in percent were calculated as $100 \times \left[b_{bp}^{fit}(\lambda) - b_{bp}^{obs}(\lambda)\right]/b_{bp}^{obs}(\lambda)$. Mean values with standard deviations are summarized in Fig. 8c for the two projects. For the ICESCAPE cruises, the fitted prediction and the observation agree within 5% for nearly all spectral bands.
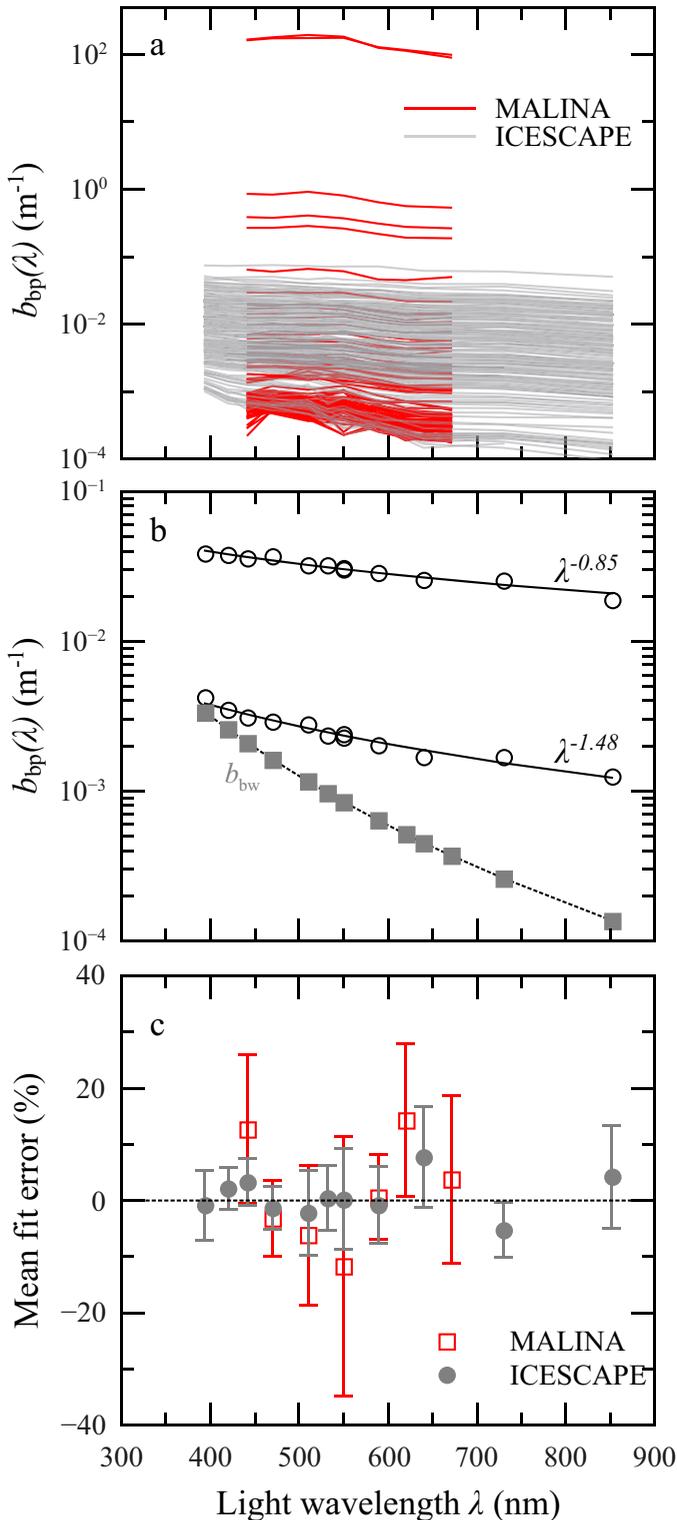
Fig. 8. **(a)** All measured spectra of the particle backscattering coefficient, $b_{bp}(\lambda)$, obtained during the MALINA and ICESCAPE cruises. **(b)** Two example $b_{bp}(\lambda)$ spectra from the ICESCAPE 2011 cruise illustrating the discrete measurements in eleven spectral bands and the spectral dependency calculated from a power law fit. Measurements from two independent instruments are shown at 550 nm for each spectra. The average value of the molecular water backscattering coefficient, $b_{bw}(\lambda)$, for the combined cruises is also depicted. **(c)** Mean and standard deviations of the percentage difference between measured and fitted $b_{bp}(\lambda)$ in each spectral band. Results are shown individually for the two projects.
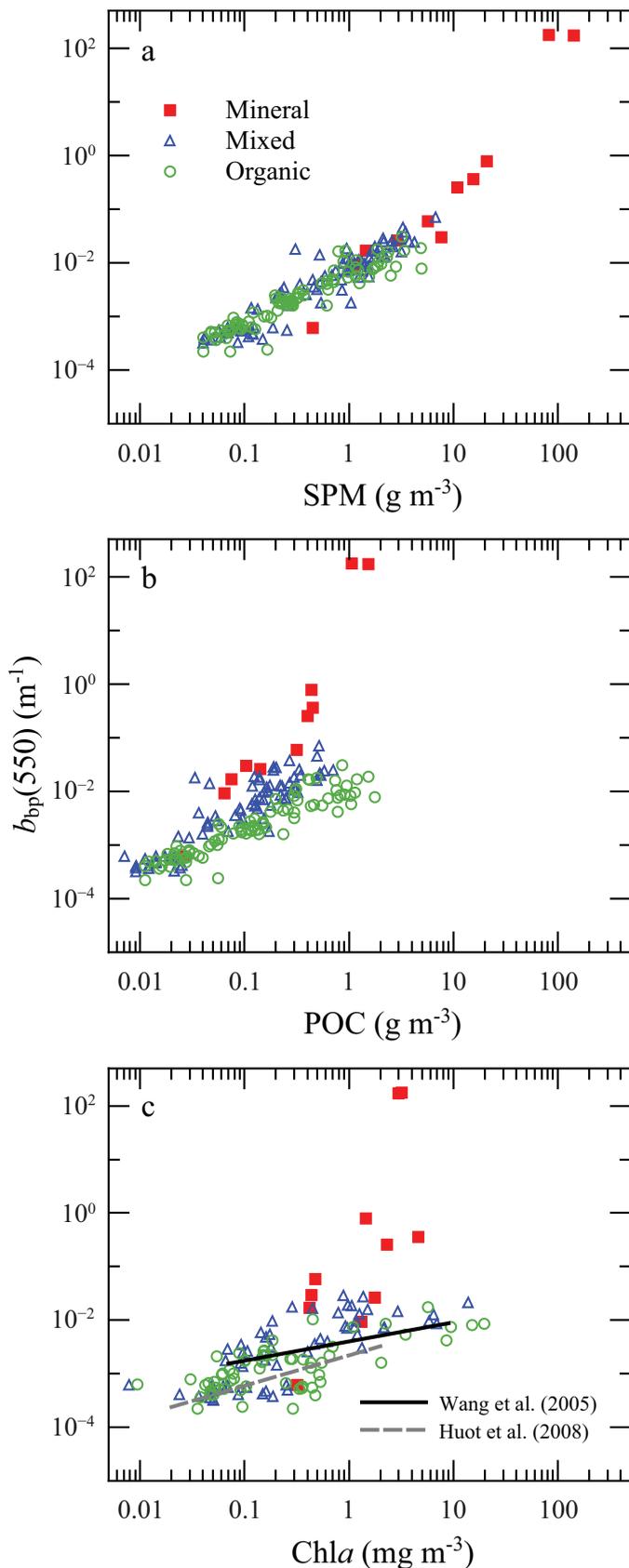
Table 1. Summary of fitted regression coefficients and error statistics for the relationships between the particle backscattering coefficient at 550 nm (in units of m^{-1}) and three measures of particle mass concentration. Data were fit to the power function $b_{bp}(550) = k_1 \, X^{k_2}$, where X is the measure of particle mass concentration as indicated in the table, using a Model II linear regression on $\log_{10}$-transformed variables. Separate fits were also determined for individual compositional classes as defined by the POC/SPM ratio. All regressions are significant (F-test, $p < 0.05$), standard error estimates are given in parentheses for the fitted coefficients. The determination coefficient, R^2, and the root mean square error, RMSE, are calculated from the $\log_{10}$-transformed variables. n represents the number of observations included in the regression.

Class	k_1	k_2	R^2	RMSE	n
$X = $ SPM [g m^{-3}]					
Mineral	0.004(1.42)	1.67(0.19)	0.91	0.30	9
Mixed	0.009(1.05)	1.09(0.04)	0.85	0.24	123
Organic	0.006(1.04)	0.93(0.03)	0.90	0.17	142
All data	0.008(1.04)	1.06(0.02)	0.88	0.23	274
$X = $ POC [g m^{-3}]					
Mineral	2.405(1.63)	2.14(0.23)	0.92	0.29	9
Mixed	0.096(1.16)	1.22(0.06)	0.75	0.31	123
Organic	0.016(1.08)	0.91(0.03)	0.86	0.20	142
All data	0.052(1.12)	1.18(0.05)	0.60	0.41	274
$X = $ Chl$a$ [mg m^{-3}]					
Mineral	0.043(1.87)	2.36(0.72)	0.35	0.82	9
Mixed	0.008(1.12)	0.81(0.06)	0.45	0.46	98
Organic	0.003(1.08)	0.58(0.04)	0.61	0.30	105
All data	0.006(1.09)	0.82(0.04)	0.37	0.51	212

Fits were generally poorer and exhibited wider standard deviations for the MALINA data, with average values ranging from 0.6% to 14% depending upon wavelength.

Relationships between b_{bp} and particle mass concentration

Figure 9 depicts relationships between the particulate backscattering coefficient at 550 nm, $b_{bp}(550)$, and the three measures of particle mass concentration, SPM, POC, and Chl$a$. The spectral region around 550 nm exhibits generally weak pigment absorption and this band is frequently employed in ocean color algorithms utilizing blue-to-green band ratios. In Fig. 9, the bulk compositional class of the assemblage based on the POC/SPM ratio is identified for individual points. The magnitude of $b_{bp}(550)$ was highly correlated with the particle dry mass concentration for all three cruises over a large range in SPM (Fig. 9a). For extremely

Fig. 9. Scatter plots illustrating the relationships between $b_{bp}(550)$ and concentrations of **(a)** suspended particle dry mass, **(b)** particulate organic carbon, and **(c)** chlorophyll a. In all panels, the color of each symbol corresponds to the predominant particle composition as defined by the POC/SPM ratio. Panel c also depicts two previously reported relationships from the literature.

high particle concentrations with SPM > 10 g m^{-3}, the slope of the overall relationship changes and an apparent increase is observed in the particulate backscattering coefficient per unit particle mass concentration. These particular measurements all represent surface samples obtained on the shelf near the mouth of the Mackenzie River, and the particle assemblages at these stations were predominantly inorganic with a POC/SPM ratio less than 0.04. In this highly turbid environment, the apparent increase in SPM-specific backscattering may also be subject to the effects of multiple scattering, inaccuracies in the σ-correction, or both. For the two samples with the highest values of SPM ($\sim$ 100 g m^{-3}) and b_{bp} ($\sim$ 180 m^{-1}), estimates of the optical thickness τ(660) (i.e., the product c(660)·l, where c represents the beam attenuation coefficient and l represents the geometric pathlength of the Hydroscat-6 measurement) greatly exceed the single scattering criterion (τ = 0.3) and these data were subsequently rejected from further analysis. The remaining three samples with SPM > 10 g m^{-3} and b_{bp} approaching $\sim$1 m^{-1} exhibit values of τ which are near the upper limit of this general criterion, but have been retained in the following analyses.

A power law function of the form $b_{bp}(550) = k_1$ [SPM]^{k_2} provides a good description of the relationship between the particle backscattering coefficient and SPM (Table 1). The exponent of this relationship is 1.06, indicating a nearly linear covariation, and similar to the value of 1.03 obtained for the relationship at 650 nm reported for coastal and offshore waters of Europe and French Guyana (Neukermans et al. 2012). Nearly-linear relationships between the magnitude of $b_{bp}(\lambda)$ at other wavelengths and SPM have also been reported previously (Boss et al. 2009; Martinez-Vicente et al. 2010).

Relationships between b_{bp} and SPM are expected to vary for particle assemblages with differing chemical composition or size distribution. Although a similar range of variation in $b_{bp}(550)$ is observed for all three classes in Fig. 9a, the assemblages dominated by mineral particles tend to exhibit greater values of both SPM and b_{bp}. Regression analysis performed on each subset of compositional classes indicates that the organic and mixed assemblages have similar relationships, with the power law exponent close to 1 (Table 1). In contrast, the assemblages in which mineral particles predominate exhibit a twofold increase in the regression slope, and considerably higher RMSE than the other two classes. The first observation is generally consistent with theoretical models examining the backscattering properties of individual particle components in seawater (Woźniak and Stramski 2004).

In addition to b_{bp} vs. SPM, Fig. 9 also depicts similar relationships for more specific components of the particle assemblage which are of interest to biogeochemical studies (POC, Chl$a$). Because these components represent only subsets of total particle mass, the observed relationships are generally less robust and exhibit greater scatter than observed for SPM. POC is an indicator of organic matter, including both living planktonic organisms and nonliving detritus, and thus its covariation with b_{bp} exhibits the highest correlation and the lowest observed RMSE when organic particles represent the dominant source of variability within an assemblage (Table 1). For the mixed and mineral assemblages, the increasing contribution of inorganic particles increases b_{bp} but does not contribute to POC, and a greater discrimination in the relationships of b_{bp} vs. POC for the different compositional classes is observed relative to b_{bp} vs. SPM.

The concentration of chlorophyll a is an even more specific indicator targeting pigmented phytoplankton, and commonly serves as a measure of planktonic algal biomass. Because phytoplankton chlorophyll a is a small and variable component of total particle mass, relationships between backscattering and Chl$a$ often exhibit considerable scatter (e.g., Reynolds et al. 2001; Huot et al. 2008; Antoine et al. 2011). In addition, many species of coastal phytoplankton are larger than the size range expected to have a significant contribution to b_{bp}, which would further increase uncoupling of the variables involved in this relationship. As would be anticipated, the best relationship between $b_{bp}(550)$ and Chl$a$ for our measurements is observed for organic-dominated assemblages in which phytoplankton and covarying materials are important components of the particle mass concentration (Table 1). For comparison, Fig. 9c also depicts two previously-reported relationships for these variables. The relationship by Huot et al. (2008) was reported for a transect across the South Pacific Gyre, in deep oceanic waters with little to no terrigenous influence. The power law exponent of 0.58 obtained for the organic-dominated assemblage in this study compares favorably with the value of 0.52 reported by Huot et al. (2008), with a scaling factor that differs by about 20%. Their model agrees with our measurements of organic assemblages to within 10% for low Chl$a$ (< 0.5 mg m^{-3}), but are lower by about 23% for a Chl$a$ value of 2 mg m^{-3}. The fitted power model obtained with our data is also very similar to one reported at 532 nm by Loisel et al. (2010) for an analysis of the NOMAD dataset for non-turbid waters.

Wang et al. (2005) also reported a relationship for $b_{bp}(555)$ and Chl$a$ from a study encompassing locations in the Chukchi and Beaufort Seas, a region similar to the ICESCAPE cruises. Although their relationship is reported for 555 nm, the measurements were obtained from a similar Hydroscat-6 instrument and this difference of 5 nm from our reported values is likely small because of the spectral characteristics of the source and collection optics of these instruments (see Stramski et al. 2008). The scaling factor for the Wang et al. (2005) model is intermediate between the results of our regressions for organic and mixed assemblages, but their model has a much lower exponent (0.357). The predictions of their model fall within the range of our observations, but with a tendency to predict $\sim$ 75% higher
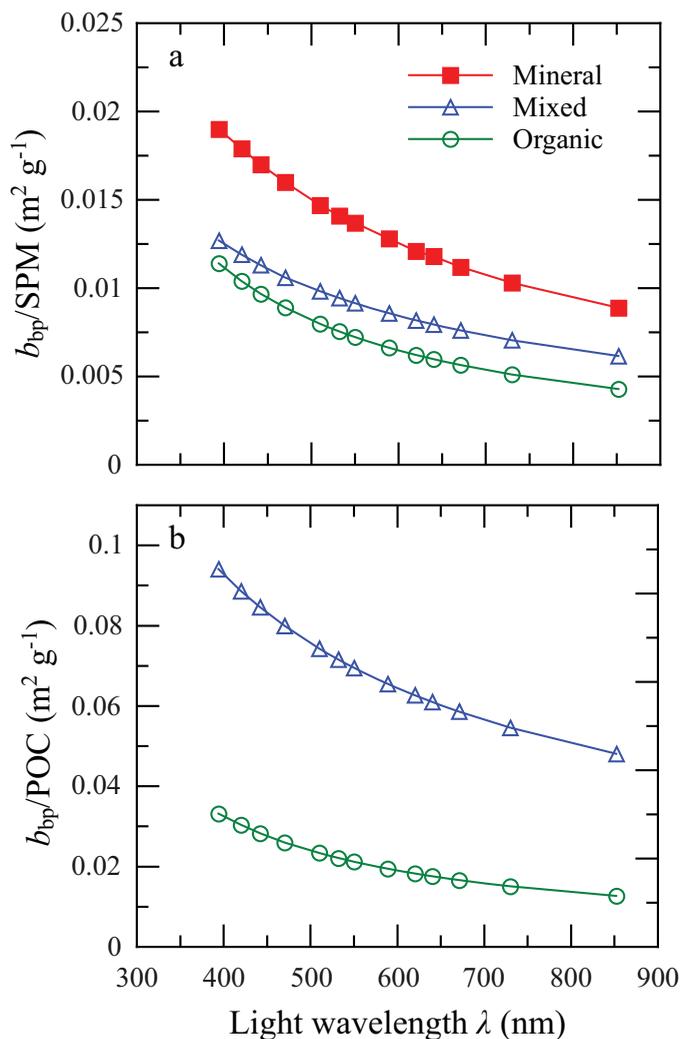
Fig. 10. (a) Spectral mean values of the SPM-specific particle backscattering coefficient obtained for each of the three compositional groups. **(b)** Similar to a, but for POC. The values for the mineral-dominated assemblage are not depicted owing to high variance around the mean.

backscattering for organic assemblages exhibiting low to moderate Chl*a* (0.1–1 mg m^{-3}). This may result from differences in the processing of backscattering measurements, or as their measurements were obtained later in the summer season (August) could reflect an increased contribution to backscattering by nonalgal particles or the predominance of smaller phytoplankton assemblages at a given Chl*a*. Their model converges with our results for organic assemblages at higher values of Chl*a* ($\sim$ 4 mg m^{-3}).

Increasing contributions of minerogenic particles to particle mass increases the backscattering coefficient independently of chlorophyll *a* concentration, leading to larger scatter and separation between assemblages of differing composition for the b_{bp} vs. Chl*a* relationship (Fig. 9c). In the case of the mineral-dominated assemblages, at any given concentration of chlorophyll *a* the observed $b_{bp}(550)$ is gen-

erally substantially higher than for organic or mixed assemblages of similar Chl*a*. The computed power function between $b_{bp}(550)$ and Chl*a* for these inorganic-dominated assemblages is still statistically significant (at $p < 0.05$) but the relationship exhibits considerable scatter with a much higher RMSE compared to all other relationships (Table 1).

Variability in mass-specific $b_{bp}(\lambda)$

The observed differences in the relationships between backscattering and the three measures of particle mass concentration (SPM, POC, Chl*a*) for different compositional assemblages can be interpreted as differences in the average mass-specific backscattering coefficient, $b_{bp}^m(\lambda)$, where *m* refers to SPM, POC, or Chl*a*. For all three proxies of mass concentration, organic-dominated assemblages exhibit the lowest average values and smallest variability of $b_{bp}^m(\lambda)$, mineral-dominated assemblages have the largest values and exhibit the highest variability, with mixed assemblages intermediate between these two.

Figure 10a illustrates spectral values of the mean SPM-specific particle backscattering coefficient, $b_{bp}^{SPM}(\lambda) = b_{bp}(\lambda)/$ SPM, for each of the three compositional groups. Because the set of measured wavelengths varies among cruises, for this analysis fitted spectra of $b_{bp}(\lambda)$ (Eq. 4) were used to extrapolate each measured spectrum to the 13 spectral bands encompassed in the entire data set prior to normalization by mass concentration and averaging. For $\lambda = 550$ nm, the average value of $b_{bp}^{SPM}(550)$ for mineral-dominated assemblages is nearly twofold higher than that observed for organic assemblages. This value of 0.0137 ($\pm$ 0.01) m^2 g^{-1} is within the range of values ($\sim$ 0.005–0.02) calculated for pure mineral particle assemblages of varying refractive index and PSDs (Woźniak and Stramski 2004), and compares favorably with those reported for field measurements of mineral-dominated assemblages in the Irish Sea (McKee and Cunningham 2006), various coastal waters of the United States of America (Snyder et al. 2008), and from Europe and French Guyana (Neukermans et al. 2012). The mean value of $b_{bp}^{SPM}(550) = $ 0.0072 ($\pm$ 0.003) m^2 g^{-1} obtained for organic-dominated assemblages also compares favorably with the values reported by the latter two studies.

A power function describing the spectral values of mean $b_{bp}^{SPM}(\lambda)$ for each of the compositional classes is given in Table 2. These relationships are tabulated to permit the estimation of mass-specific b_{bp} at an arbitrary wavelength, but should be used with caution as $b_{bp}^m(\lambda)$ can exhibit a wide range of variation even within a given class. For example, the coefficient of variation around the mean value of $b_{bp}^{SPM}(550)$ is 40% for the organic-dominated assemblage, and use of this single value for describing all samples leads to an RMSE comparable to the mean value and a median prediction error of 27% (Table 2). This range of variation and prediction error is similar at other wavelengths. The relative degree of variability for mixed assemblages is similar to the organic class,

Table 2. Fitted functions for spectra of the average SPM-specific and POC-specific particle backscattering coefficients, $b_{bp}^{SPM}(\lambda)$ and $b_{bp}^{POC}(\lambda)$ respectively, for particle assemblages representing selected compositional classes. Mean values obtained at discrete wavelengths (depicted in Fig. 10) were fitted to a power function of the form $b_{bp}^{m}(\lambda) = b_{bp}^{m}(550)\,(\lambda/550)^{k_3}$, where m is the measure of particle mass concentration as indicated in the table, $b_{bp}^{m}(550)$ is the mean value at 550 nm, and light wavelength λ is in nm. The mean and standard deviation of $b_{bp}^{m}(550)$ is given in the table. The relationships for $b_{bp}^{POC}(\lambda)$ of the mineral class, and for $b_{bp}^{Chla}(\lambda)$ of all classes, are not given owing to a very wide range of variability around the mean values and subsequent large errors in application of a single mean value. The values of RMSE for the predicted values and the median prediction difference, MPD (in percent), are given at a wavelength of 550 nm, and these values are generally representative of the entire measured spectral range from 394 nm to 852 nm. The MPD represents the median of the individual absolute percent differences (PD_i) between observed (O_i) and predicted (P_i) values of $b_{bp}^{m}(550)$, where $PD_i = 100 \times (|P_i - O_i|/O_i)$. The number of observations in each class are the same as those listed in Table 1.

Class	$b_{bp}^{m}(550)$ [m^2 g^{-1}]	k_3	RMSE [m^2 g^{-1}]	MPD [%]
$b_{bp}^{SPM}(\lambda)$ [m^2 g^{-1}]				
Mineral	0.0137(0.010)	−0.990(0.004)	0.013	43.9
Mixed	0.0091(0.006)	−0.933(0.011)	0.006	24.4
Organic	0.0072(0.003)	−1.277(0.018)	0.003	27.2
$b_{bp}^{POC}(\lambda)$ [m^2 g^{-1}]				
Mixed	0.0695(0.061)	−0.872(0.006)	0.065	49.4
Organic	0.0212(0.010)	−1.254(0.016)	0.011	31.0

but mineral-dominated assemblages exhibit even higher variability.

Compared to $b_{bp}^{SPM}(\lambda)$, values of the POC-specific particle backscattering coefficient, $b_{bp}^{POC}(\lambda)$, are naturally higher and exhibit increased separation among the three compositional classes (Fig. 10b). Values for the mineral-dominated assemblages are on average about 21-fold higher than organic-dominated ones when compared across the entire spectral range, but at each wavelength exhibit standard deviations which exceed the mean value. Because of such large variation, the use of a single mean value to represent $b_{bp}^{POC}(\lambda)$ for a mineral-dominated assemblage is not justifiable and we do not report results for this assemblage in either Fig. 10b or Table 2. For the mixed and organic compositional groups, the degree of variation around the mean value of $b_{bp}^{POC}(\lambda)$ is only slightly higher compared to that for SPM. The mean value in the green spectral range obtained for organic-dominated assemblages ($\sim$0.02 m^2 g^{-1}) is comparable to previously reported values from the open ocean waters of the Pacific and Atlantic (0.014–0.027, Stramski et al. 2008; Cetinić et al. 2012) and from the Southern Ocean (0.0054–0.022, Stramski et al. 1999, Allison et al. 2010).

As Chl$a$ comprises only a small and variable portion of total particle mass, the Chl$a$-specific particle backscattering coefficient is generally 3 orders of magnitude higher than values per unit SPM but exhibits even a greater range of variation within each compositional class. For the same reasons described with regards to $b_{bp}^{POC}(\lambda)$ for mineral assemblages, we do not report mean values of $b_{bp}^{Chla}(\lambda)$ for any of the three compositional groups in Fig. 10 or Table 2.

Spectral variability of $b_{bp}(\lambda)$

Values of the spectral slope η of particle backscattering were always negative, and ranged from −3.01 to −0.13 with a median value of −1 (Fig. 11a). The majority of the observations (80%) lie within the narrower range of −1.5 to −0.5. A general inverse relationship is observed between η and the magnitude of b_{bp} (Fig. 11b), with the flattest (least negative) slopes tending to be associated with the most turbid waters ($b_{bp}(550) > 0.01$ m^{-1}) and increasing steepness with increasingly clearer waters. Similar behavior was observed in a compilation of measurements from coastal waters by Snyder et al. (2008), who pointed out that for clear waters the total backscattering as measured with the Hydroscat instrument is dominated by the water contribution. The average value of $b_{bw}(550)$ for our dataset is indicated in Fig. 11b, and the values of the slope of particle backscattering generally decrease rapidly and become more negative when water contributes > 50% to the total b_b. In these cases, the values of b_{bw} chosen to calculate $b_{bp}(\lambda)$ can have a large effect on the computed values and spectral slope of b_{bp}, and thus the sharp decrease in η observed in increasingly clearer waters should be interpreted with some caution.

In contrast to the magnitude of b_{bp}^{m}, we do not observe systematic differences in the spectral slope of $b_{bp}(\lambda)$ associated with each compositional group (Fig. 12). The organic and mixed particle assemblages span most of the range associated with η and exhibit high variability within each group. An analysis of variance suggests that the mean value of η associated with each of these two groups, −1.26 and −1.03 respectively, are significantly different from each other ($p = 0.002$). With one exception, the mineral assemblages tend to exhibit values of η around −1 but the mean value was not statistically different from either the mixed or organic-dominated assemblages ($p \geq 0.5$). This may reflect the limited number of observations available for this group, or that mineral assemblages were generally associated with turbid environments in our dataset, or both.
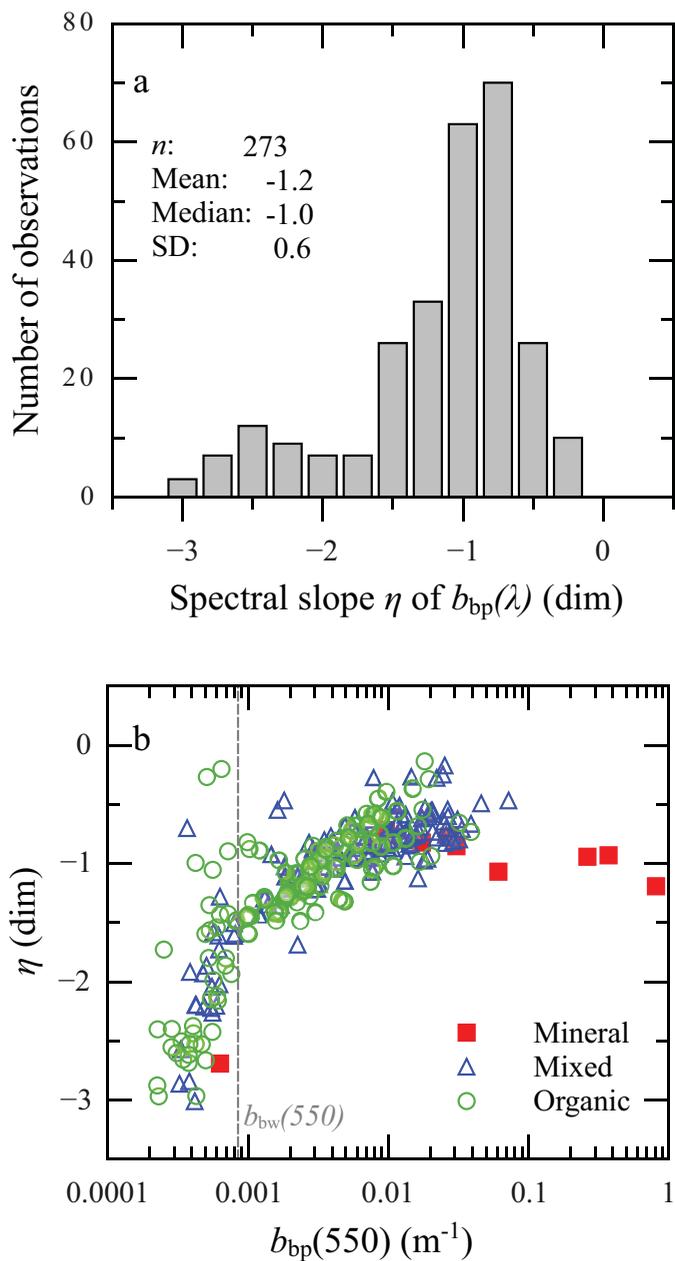
Fig. 12. Scatter plot of the relationship between the spectral slope η of $b_{bp}(\lambda)$ and the POC/SPM ratio. The three compositional groups of particle assemblages are indicated.

Fig. 11. (a) Frequency distribution of the power law exponent η representing the spectral slope of $b_{bp}(\lambda)$. **(b)** Relationship between η and $b_{bp}(550)$ for different particle compositional groups. The average value of $b_{bw}(550)$ is indicated by the vertical dashed line.

Discussion

Use of backscattering measurements to infer particle mass concentrations

Determination of the mass concentration of suspended particles in aquatic ecosystems is of direct interest to numerous basic and applied research questions. To first order, variations in the IOPs of seawater such as the beam attenuation or scattering coefficient are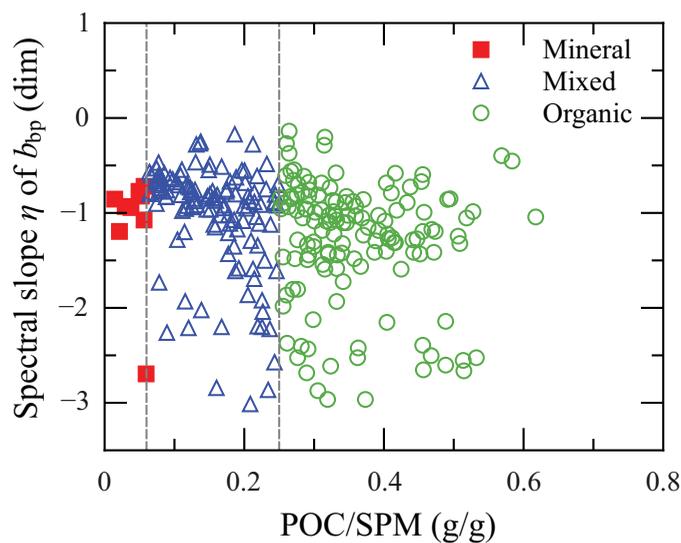 driven by the concentration of suspended particles, and thus these quantities have long been used as proxies for particle mass concentration. Second order effects which influence the optical behavior of the bulk particle assemblage, such as changes in the relative composition of particles comprising the assemblage or the physical characteristics of these particles, contribute to the uncertainties associated in the application of measured relationships across different environments.

We observed systematic differences in the mass-specific particle backscattering coefficient for three compositional groups defined by the POC/SPM ratio, an indicator of the relative contributions of organic and inorganic particles to particle mass concentration. These changes are generally consistent with observations of variation in apparent particle density and PSD associated with each group. Of the three groups, mineral-dominated assemblages exhibited the steepest PSDs with an associated greater contribution of smaller particles to metrics such as total particle projected area, and a generally higher mean apparent particle density that is consistent with a greater role of particles with increased refractive index. In contrast, for assemblages in which organic particles predominate the PSD tended to be flatter with a corresponding increase in the role of large particles, and apparent particle densities were markedly lower. As a result of these differences, the average mass-specific $b_{bp}(\lambda)$ coefficient of mineral assemblages was nearly twice that of organic assemblages. Mixed assemblages which exhibit characteristics of both inorganic and organic particles fell in between these two extremes.

Overall these results are consistent with modeling studies of idealized particle assemblages in which all particles are the same composition and shape, and only the particle
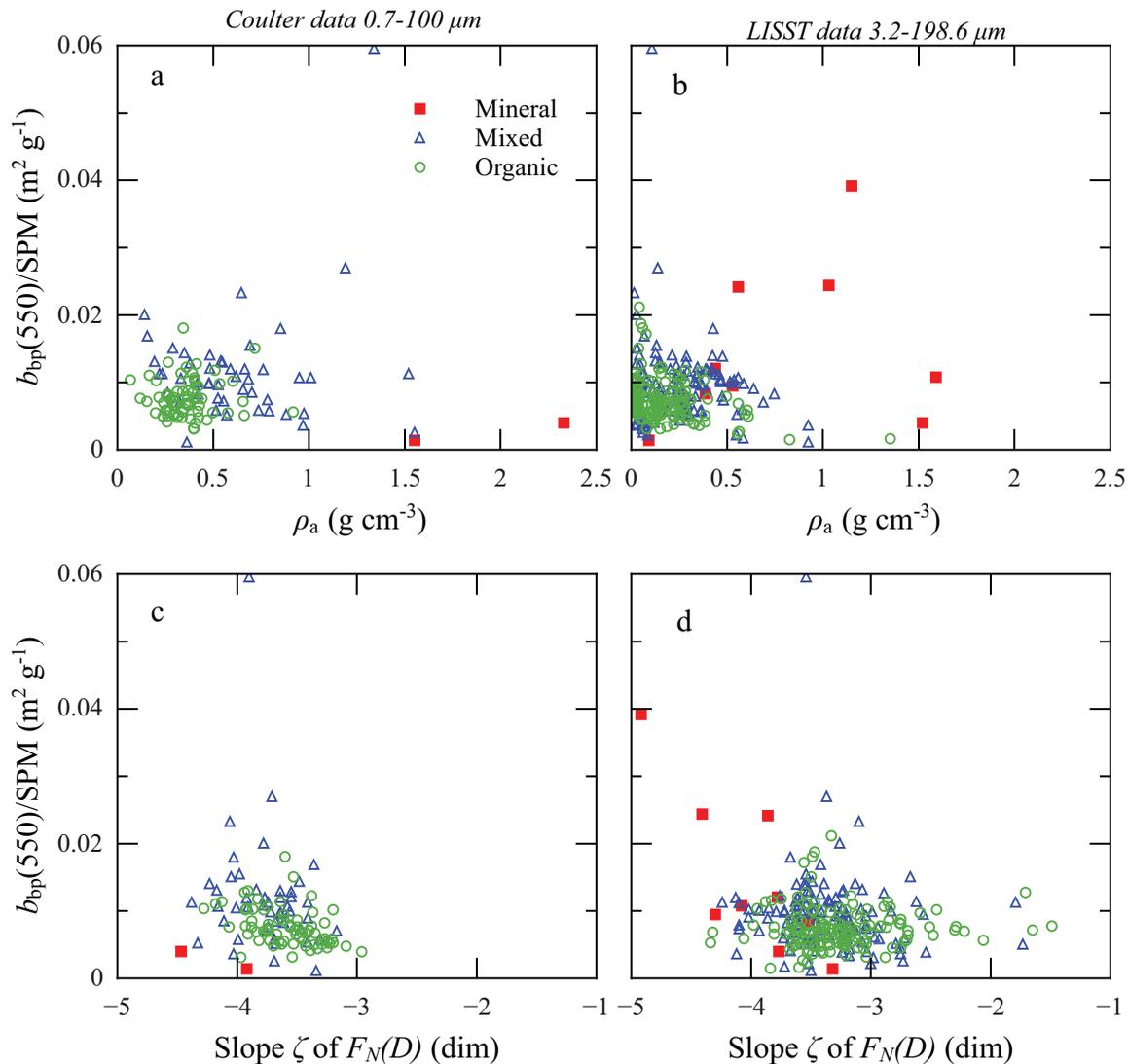
Fig. 13. Scatter plots depicting relationships between the SPM-specific particle backscattering coefficient obtained for each of the three compositional groups with **(a, b)** apparent mean particle density, ρ_a, and **(c, d)** the slope parameter ζ of the particle number size distribution. Panels a and c represent measures of ρ_a and ζ determined from Coulter counter measurements, whereas panels b and d represent values determined with the LISST.

refractive index or PSD is varied. These studies suggest that increasing particle refractive index or the steepness of the PSD lead to increases in bulk values of the mass-specific scattering or backscattering coefficient (e.g., Babin et al. 2003; Woźniak and Stramski 2004). As these characteristics of the particle assemblage generally covary in our dataset (Fig. 7), it is difficult to separate their individual contributions to the observed optical differentiation. Scatter plots depicting the individual relationships between observed values of $b_{bp}^{SPM}(550)$ and estimated values of apparent particle density or the slope of the PSD show only weak trends (Fig. 13), with some indication that the relationships are stronger for the mineral-dominated assemblages than for the other compositional groups. These weak relationships may reflect inherent experimental limitations in the determination of

these indicators, for example the finite and differing size ranges of the PSD used in determination of SPM, the particle volume concentration, and the PSD slope. It is also likely that, unlike idealized models, natural particle assemblages exhibit considerable variability in the partitioning of particle mass, refractive index, and shape among different portions of the PSD. Such variability may obscure the simple relationships expected from modeling studies, and even dampen the expected variability in $b_{bp}^{SPM}(\lambda)$ among assemblages of differing physical characteristics.

Our results indicate that the particle backscattering coefficient is well-correlated with total suspended particle mass concentration in Arctic coastal and oceanic waters. The predictive relationship between $b_{bp}(550)$ and SPM combined for all measurements in this dataset is slightly more robust than

Table 3. Fitted regression coefficients and error statistics for the prediction of SPM and POC from measurements of the particle backscattering coefficient at 550 nm, $b_{bp}(550)$, in units of m^{-1}. The coefficients of the power function $Y = k_4\, b_{bp}(550)^{k_5}$, where Y is the measure of particle mass concentration as indicated in the table, were determined using a Model I linear regression on $\log_{10}$-transformed variables. Separate fits are also given for selected individual compositional classes as defined by the POC/SPM ratio. Standard error estimates are given in parentheses for the fitted coefficients. The determination coefficient R^2 and RMSE are calculated from the $\log_{10}$-transformed variables, and all regressions are significant (*F*-test, $p < 0.05$). The remaining descriptors of error have been calculated from the non-transformed data. In addition to MPD, additional error statistics include the median ratio of observed to predicted values (MR), and the mean normalized bias (MNB) in percent representing the average relative difference between predicted and observed values.

Class	k_4	k_5	R^2	RMSE	MPD [%]	MR	MNB [%]	n
Y = SPM [g m^{-3}]								
Mineral	24.8 (1.3)	0.57 (0.07)	0.91	0.18	11.2	1.07	6.3	9
Mixed	53.7 (1.2)	0.85 (0.03)	0.85	0.22	26.5	1.01	13.3	123
Organic	160.4 (1.2)	1.02 (0.03)	0.90	0.18	22.9	1.02	8.6	142
All data	96.9 (1.1)	0.95 (0.02)	0.88	0.21	28.5	1.06	12.5	274
Y = POC [g m^{-3}]								
Mixed	4.0 (1.2)	0.72 (0.04)	0.77	0.24	37.9	1.04	17.7	123
Organic	57.0 (1.2)	1.02 (0.03)	0.87	0.22	28.7	1.02	12.3	142

that observed for the beam attenuation coefficient, as has been noted in other studies (Boss et al. 2009; Neukermans et al. 2012). These results suggest that SPM in this environment can be predicted from measurements of $b_{bp}(\lambda)$ with a median prediction difference (MPD) of about 29%, assuming no a priori knowledge of the particle assemblage (Table 3). MPD represents a measure of random error, while the median ratio of predicted to observed values (MR) and the mean normalized bias (MNB) are also provided in the table as indicators of systematic bias. These error statistics are generally improved relative to the combined model if separate predictive relationships are established for each compositional group of particle assemblage.

The accuracy of backscattering-based predictive relationships is degraded when more specific components of particle mass, such as the concentrations of particulate organic carbon or chlorophyll *a*, are considered. These quantities are often of more direct interest to biogeochemical studies than total particle mass concentration, but their contribution to both SPM and $b_{bp}(\lambda)$ can be highly variable within the ocean. In consequence, there are generally higher uncertainties associated with using empirical relationships between these measures of particle mass concentration and the backscattering coefficient. Table 3 also provides relationships for the estimation of POC from $b_{bp}(550)$ for the organic-dominated and mixed compositional groups. As indicated in Fig. 9, separation in the relationships between POC and Chl*a* with the backscattering coefficient among the compositional groups is higher relative to SPM, and thus the use of separate predictive relationships for each particle assemblage has an even greater influence on improving prediction accuracy. However, because of the large variability in mean mass-specific values of $b_{bp}^{POC}(\lambda)$ for the mineral-dominated group and of $b_{bp}^{Chla}(\lambda)$ for all compositional groups, the predictive

relationships for these variables are associated with high uncertainties even with the use of separate relationships. These relationships are therefore not reported in Table 3.

Woźniak et al. (2010) demonstrated that in California coastal surface waters where particle assemblages vary throughout the year, partitioning the assemblages into basic groups based on bulk composition resulted in improved predictive relationships between IOPs and metrics of particle concentration and size. Similar results are also obtained in the present study, in which the relationships between $b_{bp}(\lambda)$ and particle mass concentration are generally improved for specific assemblages defined by the POC/SPM ratio compared to the combined dataset. These observations suggest that the incorporation of class-specific models to estimate various measures of particle mass concentration from backscattering measurements can lead to improved predictive capabilities with reduced uncertainties. Implementation of such an approach requires having information about the particle assemblage present during measurement. In some cases reasonable assumptions regarding the dominant compositional class can be made based on general environmental knowledge, for example the likely predominance of mineral materials in turbid river discharges or of organic materials in blooms of planktonic organisms. A more general approach would be to develop and utilize other measured optical characteristics as indicators of the particle assemblage, for which appropriate relationships between $b_{bp}(\lambda)$ and particle mass could be subsequently applied. For example, a multistep algorithm approach was demonstrated in the Woźniak et al. (2010) study which utilized the particulate absorption ratio at two bands to first estimate the bulk compositional class of the particles, followed by the application of class-specific algorithms to determine SPM or POC. In an alternative but conceptually similar approach, Neukermans et al. (2016)
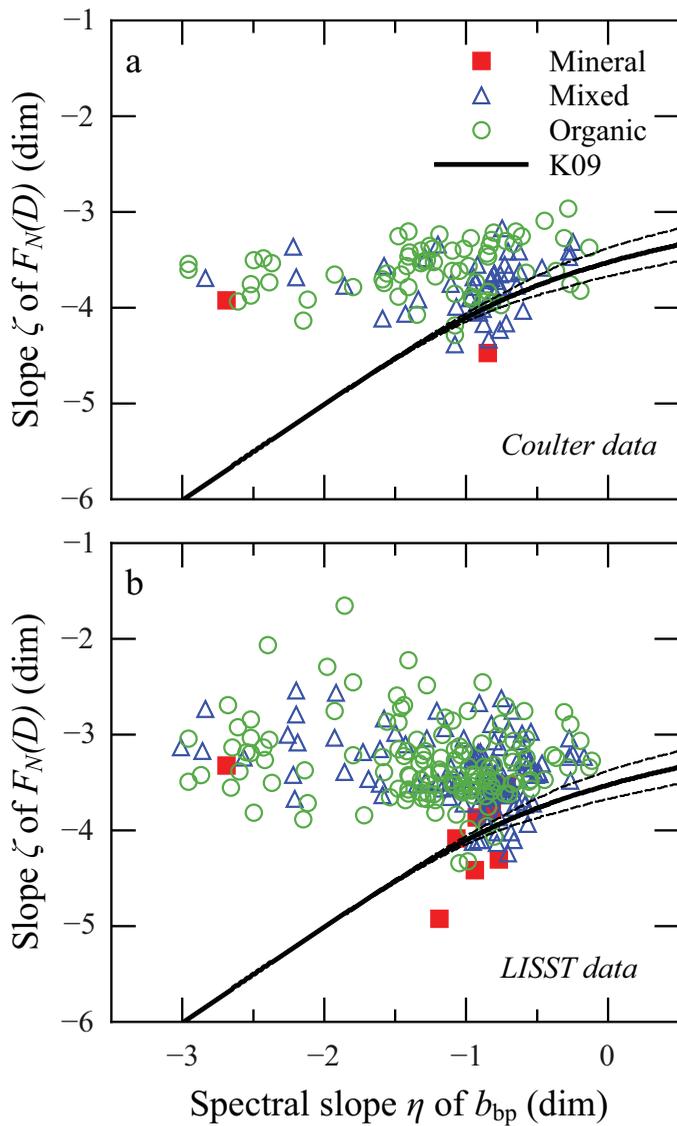
Fig. 14. Relationship between the spectral slope η of $b_{bp}(\lambda)$ and the slope parameter ζ of the particle number distribution derived from either **(a)** the Coulter counter or **(b)** the LISST. The solid line represents the calculated relationship from the model of Kostadinov et al. (2009).

identified and classified specific particle assemblages through a hierarchical cluster analysis of the particulate backscattering to absorption ratio, and demonstrated a potential for improved estimates of SPM from $b_{bp}(\lambda)$ through the application of cluster-specific relationships. We note that the particulate absorption coefficient utilized in both of these approaches can be determined from in situ measurements or derived from satellite ocean color.

Spectral slope of particle backscattering as an indicator of particle size distribution

The spectral behavior of $b_{bp}(\lambda)$ has also been suggested as a potential optical indicator that can provide additional information on the size distribution of particles suspended in seawater. Theoretically, the spectral dependence of the particle scattering coefficient is sensitive to the slope of the PSD (Morel 1976), and results from modeling studies (Stramski et al. 2001; Woźniak and Stramski 2004) as well as observations from field and satellite measurements (Reynolds et al. 2001; Loisel et al. 2006; Slade and Boss 2015) have suggested a general correspondence between the spectral slope of the particle backscattering coefficient, η, and the proportional contributions of large and small particles to total particle concentration. Using Mie scattering theory, Kostadinov et al. (2009) modeled the relationship between η and the slope of the particle number size distribution, ζ, for different combinations of particle refractive index and PSDs. Based on these calculations, they proposed an operational algorithm to predict the magnitude and shape of $F_N(D)$ based on η (hereafter referred to as the K09 model). The use of this model in conjunction with satellite-retrieved estimates of η has been used to examine the spatial and temporal distribution of the PSD and the size structure of phytoplankton at global scales (Kostadinov et al. 2009; Kostadinov et al. 2010).

Using the contemporaneous measurements of backscattering and PSD from this study, we examined the relationship between measured values of the spectral slope η of $b_{bp}(\lambda)$ and the slope ζ of $F_N(D)$ determined from either the LISST or Coulter measurements (Fig. 14). Our observations suggest little to no correlation between these two quantities, either overall or within specific compositional classes. For comparison, the relationship predicted by the K09 model is also shown in Fig. 14. For a given value of the spectral slope η, the measured slope of the particle number distribution exhibits a strong tendency to be less negative (i.e., flatter) than the model prediction throughout the range of observations. The divergence is greatest for the steepest slopes of $b_{bp}(\lambda)$, in which the model predicts very steep slopes of $F_N(D)$ ($\zeta < -4.5$) that are generally not observed in either the LISST or Coulter measurements.

In addition to the slope ζ of particle number distribution, the K09 model also utilizes the value of η to estimate the ratio of $b_{bp}(440)/N_o$, where N_o is the differential particle concentration at a reference diameter. This quantity is used to scale the magnitude of the PSD, and together with the slope ζ provides a quantitative description of the $F_N(D)$. A comparison of this scaling factor with our measured values suggests that the model on average underpredicts concentration at the reference diameter by more than 50% (not shown).

In general, our measurements from Arctic waters suggest that despite large changes in η there is no clear relationship with changes in the overall slope ζ of the particle number distribution. There are several potential reasons for this lack of correspondence between modeled behavior and field observations. The Mie scattering calculations employ the simplifying assumptions of homogenous spherical particles, which is a poor description of many particles in the natural

marine environment. The use of an idealized single-slope power law model over the entire optically-relevant size range of parameters to parameterize the particle number distribution also has known limitations, particularly in waters subject to the occurrence of rapidly-changing populations of plankton species (Reynolds et al. 2010).

We acknowledge that measurement limitations may also contribute to the apparent lack of coherence. In this study, the general trends we observe are seen in two independent measures of the PSD which utilize very different principles of measurement and cover different portions of the PSD. Both techniques, however, suffer from the inability to measure particles in submicron particle size range, which has been suggested to be an important contributor to b_{bp} in oceanic waters (Stramski and Kiefer 1991; Stramski and Woźniak 2005).

Implications

The use of optical sensors to obtain information on the various constituents of seawater has greatly extended the observational capabilities for studies of the marine environment. Optical measurements possess a major advantage in the ability to make measurements rapidly and at higher temporal and spatial resolution compared to direct laboratory methods. Such capabilities are particularly important in regions where direct observations are limited, such as the Arctic Ocean and surrounding seas.

For studies of suspended particles in seawater, the beam attenuation coefficient has typically been utilized as this measurement is routinely incorporated on standard CTD packages deployed by research vessels. However, transmissometers are not well suited to many of the current generation of autonomous vehicles (e.g., gliders, floats) used for oceanic studies, and instead these platforms typically employ commercially-available sensors which provide the scattering coefficient at backward angles. Additionally, the backscattering coefficient is directly linked to the remote-sensing reflectance signal measured by an above-water sensor, and several inverse models have been developed to estimate $b_{bp}(\lambda)$ from such measurements (Loisel and Stramski 2000; Lee et al. 2002; Maritorena et al. 2002) and evaluated in Arctic waters (Zheng et al. 2014). Backscattering measurements are thus likely to be an increasingly used observational tool in future research. As variability in the magnitude and spectral behavior of the backscattering coefficient is theoretically sensitive to the abundance as well as characteristics of particles present in the interrogated volume, interpretation of this optical signal represents a major challenge but also a potential opportunity for obtaining a wealth of information. Because of the restrictive assumptions required by theoretical studies, empirical field observations are a continued necessity for an improved understanding of these relationships.

Our results indicate that the magnitude of the particle backscattering coefficient can serve as useful proxy for various measures of particle mass concentration, particularly in environment where variations in particle mass are primarily restricted to changes in the abundance of similar types of particles. However, the uncertainties become much greater in complex waters which exhibit varying mixtures of diverse particle types. Prior knowledge of relatively simple information regarding the average bulk composition of the suspended particle assemblage coupled with the use of assemblage-specific relationships can in many cases lead to much improved estimates of particle mass concentrations, or at least identify situations where the application of any given model is unlikely to perform well. We believe that this approach is not limited to the Arctic, but is likely to prove beneficial in many aquatic ecosystems where inorganic and planktonic particles represent varying proportions of the suspended particle pool.

Within our dataset, the spectral dependency of $b_{bp}(\lambda)$ is generally well-described by a power law function throughout the visible spectral range, with the possible exception of bands located in or near regions of strong absorption features. Values of the spectral slope exponent η exhibit an ~20-fold variability, although the majority of observations are limited to a more restricted range. Surprisingly, variability in the spectral slope of particle backscattering in our dataset appear to be most closely associated with changes in seawater turbidity (Fig. 11b), or alternatively with the bulk particle mass concentration (via Fig. 9a). This overall pattern is qualitatively consistent with ocean color observations from satellite sensors (Loisel et al. 2006), and has been interpreted as representing changes in the PSD across oceanic regimes. However, in contrast to this hypothesis and the predictions of theoretical models, the observed variability of η in our dataset does not seem to be correlated in any significant way with the slope of the PSD determined from two independent methods of measurement. Such a result implies that appropriate caution should be exercised when using the spectral dependence of particle backscattering to infer patterns of PSD or phytoplankton community composition, especially in the complex waters of the Arctic Ocean and adjacent seas.

References

Aas, E. 1996. Refractive index of phytoplankton derived from its metabolite composition. J. Plankton Res. **18**: 2223–2249.

Agrawal, Y. C., and H. C. Pottsmith. 2000. Instruments for particle size and settling velocity observations in sediment transport. Mar. Geol. **168**: 89–114. doi:10.1016/S0025-3227(00)00044-X

Agrawal, Y. C., A. Whitmire, O. A. Mikkelsen, and H. C. Pottsmith. 2008. Light scattering by random shaped particles and consequences of measuring suspended sediments by laser diffraction. J. Geophys. Res. **113**: C04023. doi:10.1029/2007JC004403

Allison, D. B., D. Stramski, and B. G. Mitchell. 2010. Empirical ocean color algorithms for estimating particulate

organic carbon in the Southern Ocean. J. Geophys. Res. **115**: C10044. doi:10.1029/2009jc006040

Andrews, S., D. Nover, and S. G. Schladow. 2010. Using laser diffraction data to obtain accurate particle size distributions: The role of particle composition. Limnol. Oceanogr.: Methods **8**: 507–526. doi:10.4319/lom.2010.8.507

Andrews, S. W., D. M. Nover, K. E. Reardon, J. E. Reuter, and S. G. Schladow. 2011. The influence of ambient light intensity on in situ laser diffractometers. Water Resour. Res. **47**: W06509. doi:10.1029/2010WR009841

Antoine, D., and others. 2011. Variability in optical particle backscattering in contrasting bio-optical oceanic regimes. Limnol. Oceanogr. **56**: 955–973. doi:10.4319/lo.2011.56.3.0955

Arrigo, K. R. 2015. Impacts of climate on ecosystems and chemistry of the Arctic Pacific Environment (ICESCAPE). Deep-Sea Res. Part II Top. Stud. Oceanogr. **118**, Part A: 1–6. doi:10.1016/j.dsr2.2015.06.007

Arrigo, K. R., and others. 2014. Phytoplankton blooms beneath the sea ice in the Chukchi sea. Deep-Sea Res. Part II Top. Stud. Oceanogr. **105**: 1–16. doi:10.1016/j.dsr2.2014.03.018

Babin, M., A. Morel, V. Fournier-Sicre, F. Fell, and D. Stramski. 2003. Light scattering properties of marine particles in coastal and open ocean waters as related to the particle mass concentration. Limnol. Oceanogr. **48**: 843–859. doi:10.4319/lo.2003.48.2.0843

Bader, H. 1970. The hyperbolic distribution of particle sizes. J. Geophys. Res. **75**: 2822–2830. doi:10.1029/JC075i015p02822

Behrenfeld, M. J., E. S. Boss, D. A. Siegel, and D. M. Shea. 2005. Carbon-based ocean productivity and phytoplankton physiology from space. Global Biogeochem. Cycles **19**: 1–14. doi:10.1029/2004GB002299

Berry, L.G., and B. Mason. 1959. Mineralogy: Concepts, descriptions, determinations. Freeman.

Boss, E. S., and others. 2009. Comparison of inherent optical properties as a surrogate for particulate matter concentration in coastal waters. Limnol. Oceanogr.: Methods **7**: 803–810. doi:10.4319/lom.2009.7.803

Boss, E., and M. Behrenfeld. 2010. In situ evaluation of the initiation of the North Atlantic phytoplankton bloom. Geophys. Res. Lett. **37**: L18603. doi:10.1029/2010GL044174

Bowers, D. G., K. M. Braithwaite, W. A. M. Nimmo-Smith, and G. W. Graham. 2009. Light scattering by particles suspended in the sea: The role of particle size and density. Cont. Shelf Res. **29**: 1748–1755. doi:10.1016/j.csr.2009.06.004

Briggs, N., M. J. Perry, I. Cetinić, C. Lee, E. D'Asaro, A. M. Gray, and E. Rehm. 2011. High-resolution observations of aggregate flux during a sub-polar North Atlantic spring bloom. Deep-Sea Res., Part I **58**: 1031–1039.

Buiteveld, H., J. H. M. H. M. Hakvoort, and M. Donze. 1994. The optical properties of pure water. Proc. SPIE 2258, Ocean Optics XII, 174. doi:10.1117/12.190060

Cetinić, I., M. J. Perry, N. T. Briggs, E. Kallin, E. A. D'Asaro, and C. M. Lee. 2012. Particulate organic carbon and inherent optical properties during 2008 North Atlantic Bloom Experiment. J. Geophys. Res. **117**: C06028. doi:10.1029/2011JC007771

Cota, G. F., W. G. Harrison, T. Platt, S. Sathyendranath, and V. Stuart. 2003. Bio-optical properties of the Labrador Sea. J. Geophys. Res. **108**: 3228. doi:10.1029/2000JC000597C7

Dana, D. R., and R. A. Maffione. 2002. Determining the backward scattering coefficient with fixed-angle backscattering Sensors—revisited. Ocean Optics XVI, Santa Fe, New Mexico, November 18–22.

Darby, D. A., W. B. Myers, M. Jakobsson, and I. Rigor. 2011. Modern dirty sea ice characteristics and sources: The role of anchor ice. J. Geophys. Res. **116**: C09008. doi:10.1029/2010JC006675

Downing, J. 2006. Twenty-five years with OBS sensors: The good, the bad, and the ugly. Cont. Shelf Res. **26**: 2299–2318. doi:10.1016/j.csr.2006.07.018

Fujiwara, A., T. Hirawake, K. Suzuki, and S. Saitoh. 2011. Remote sensing of size structure of phytoplankton communities using optical properties of the Chukchi and Bering Sea shelf region. Biogeosciences **8**: 3567–3580. doi:10.5194/bg-8-3567-2011

Huot, Y., A. Morel, M. S. Twardowski, D. Stramski, and R. A. Reynolds. 2008. Particle optical backscattering along a chlorophyll gradient in the upper layer of the eastern South Pacific Ocean. Biogeosciences **5**: 495–507. doi:10.5194/bg-5-495-2008

IOCCG. 2015. Ocean colour remote sensing in polar seas. In M. Babin, K. Arrigo, S. Bélanger and M-H. Forget [eds.], IOCCG Report Series, No. 16, International Ocean Colour Coordinating Group.

Jonasz, M., and G. Fournier. 2007. Light scattering by particles in water: Theoretical and experimental foundations, 1st ed. Elsevier.

Knap, A., A. Michaels, A. Close, H. Ducklow, and A. Dickson. 1996. Protocols for the Joint Global Ocean Flux Study (JGOFS) core measurements, JGOFS Report Nr. 19 (Reprint of the IOC Manuals and Guides No. 29, UNESCO, Paris, 1994), 170 pp.

Kostadinov, T. S., D. A. Siegel, and S. Maritorena. 2009. Retrieval of the particle size distribution from satellite ocean color observations. J. Geophys. Res. **114**: C09015. doi:10.1029/2009JC005303

Kostadinov, T. S., D. A. Siegel, and S. Maritorena. 2010. Global variability of phytoplankton functional types from space: Assessment via the particle size distribution. Biogeosciences **7**: 3239–3257. doi:10.5194/bg-7-3239-2010

Lee, Z., K. L. Carder, and R. A. Arnone. 2002. Deriving inherent optical properties from water color: A multiband

quasi-analytical algorithm for optically deep waters. Appl. Optics **41**: 5755–5772. doi:10.1364/AO.41.005755

Lide, D. R. 2001. CRC handbook of physics and chemistry, 82nd ed. CRC Press.

Loisel, H., and D. Stramski. 2000. Estimation of the inherent optical properties of natural waters from the irradiance attenuation coefficient and reflectance in the presence of Raman scattering. Appl. Opt. **39**: 3001–3011. doi:10.1364/AO.39.003001

Loisel, H., J.-M. Nicolas, A. Sciandra, D. Stramski, and A. Poteau. 2006. Spectral dependency of optical backscattering by marine particles from satellite remote sensing of the global ocean. J. Geophys. Res. **111**: C09024. doi:10.1029/2005JC003367

Loisel, H., B. Lubac, D. Dessailly, L. Duforet-Gaurier, and V. Vantrepotte. 2010. Effect of inherent optical properties variability on the chlorophyll retrieval from ocean color remote sensing: an in situ approach. Opt. Express **18**: 20949–20959. doi:10.1364/OE.18.020949

Maffione, R. A., and D. R. Dana. 1997. Instruments and methods for measuring the backward-scattering coefficient of ocean waters. Appl. Opt. **36**: 6057–6067. doi:10.1364/AO.36.006057

Maritorena, S., D. A. Siegel, and A. R. Peterson. 2002. Optimization of a semianalytical ocean color model for global-scale applications. Appl. Opt. **41**: 2705–2714. doi:10.1364/AO.41.002705

Martinez-Vicente, V., G. Dall'Olmo, G. Tarran, E. Boss, and S. Sathyendranath. 2013. Optical backscattering is correlated with phytoplankton carbon across the Atlantic Ocean. Geophys. Res. Lett. **40**: 1154–1158. doi:10.1002/grl.50252

Martinez-Vicente, V., P. E. Land, G. H. Tilstone, C. Widdicombe, and J. R. Fishwick. 2010. Particulate scattering and backscattering related to water constituents and seasonal changes in the Western English Channel. J. Plankton Res. **32**: 603–619. doi: 10.1093/plankt/fbq013

Matsuoka, A., A. Bricaud, R. Benner, J. Para, R. Sempéré, L. Prieur, S. Bélanger, and M. Babin. 2012. Tracing the transport of colored dissolved organic matter in water masses of the Southern Beaufort Sea: Relationship with hydrographic characteristics. Biogeosciences **9**: 925–940.

McKee, D., and A. Cunningham. 2006. Identification and characterisation of two optical water types in the Irish Sea from in situ inherent optical properties and seawater constituents. Estuar. Coast. Shelf Sci. **68**: 305–316. doi:10.1016/j.ecss.2006.02.010

Mitchell, B. G. 1992. Predictive bio-optical relationships for polar oceans and marginal ice zones. J. Marine. Syst. **3**: 91–105. doi:10.1016/0924-7963(92)90032-4

Morel, A. 1974. Optical properties of pure water and pure sea water, p. 1–24. *In* N. G. Jerlov and E. Steeman Nielsen [eds.], Optical aspects of oceanography. Academic.

Morel, A. 1976. Diffusion de la lumière par les eaux de mer; résultats expérimentaux et approche théorique. AGARD Lect. Ser., 3.1.1.–3.1.76.

Morel, A., and A. Bricaud. 1981. Theoretical results concerning the optics of phytoplankton, with special reference to remote sensing applications, p. 313–327. *In* Proceedings of COSPAR/SCOR/IUCRM Symposium Oceanography from Space. Plenum.

Neukermans, G., H. Loisel, X. Meriaux, R. Astoreca, and D. McKee. 2012. In situ variability of mass-specific beam attenuation and backscattering of marine particles with respect to particle size, density, and composition. Limnol. Oceanogr. **57**: 124–144. doi:10.4319/lo.2011.57.1.0124

Neukermans, G., R. A. Reynolds, and D. Stramski. 2014. Contrasting inherent optical properties and particle characteristics between an under-ice phytoplankton bloom and open water in the Chukchi Sea. Deep-Sea Res. Part II Top. Stud. Oceanogr. **105**: 59–73. doi:10.1016/j.dsr2.2014.03.014

Neukermans, G., R. A. Reynolds, and D. Stramski. 2016. Optical classification and characterization of marine particle assemblages within the western Arctic Ocean. Limnol. Oceanogr. doi:10.1002/lno.10316

Parsons, T. R., Y. Maita, and C. M. Lalli. 1984. A manual of chemical and biological methods for seawater analysis. Elsevier.

Ras, J., J. Uitz, and H. Claustre. 2008. Spatial variability of phytoplankton pigment distributions in the Subtropical South Pacific Ocean: Comparison between in situ and modelled data. Biogeosciences **5**: 353–369. doi:10.5194/bg-5-353-2008

Reynolds, R. A., D. Stramski, and B. G. Mitchell. 2001. A chlorophyll-dependent semianalytical reflectance model derived from field measurements of absorption and backscattering coefficients within the Southern Ocean. J. Geophys. Res. **106**: 7125–7138. doi:10.1029/1999JC000311

Reynolds, R. A., D. Stramski, V. M. Wright, and S. B. Woźniak. 2010. Measurements and characterization of particle size distributions in coastal waters. J. Geophys. Res. **115**: C08024. doi:10.1029/2009JC005930

Ricker, W. E. 1973. Linear regressions in fishery research. J. Fish. Res. Board Can. **30**: 409–434. doi:10.1139/f73-072

Slade, W. H., and E. Boss. 2015. Spectral attenuation and backscattering as indicators of average particle size. Appl. Opt. **54**: 7264–7277. doi:10.1364/AO.54.007264

Snyder, W., and others. 2008. Optical scattering and backscattering by organic and inorganic particulates in U.S. coastal waters. Appl. Opt. **47**: 666–677. doi:10.1364/AO.47.000666

Stramski, D., and D. A. Kiefer. 1991. Light scattering by microorganisms in the open ocean. Prog. Oceanogr. **28**: 343–383. doi:10.1016/0079-6611(91)90032-H

Stramski, D., R. A. Reynolds, M. Kahru, and B. G. Mitchell. 1999. Estimation of particulate organic carbon in the ocean from satellite remote sensing. Science **285**: 239–242. doi:10.1126/science.285.5425.239

Stramski, D., A. Bricaud, and A. Morel. 2001. Modeling the inherent optical properties of the ocean based on the detailed composition of the planktonic community. Appl. Opt. **40**: 2929–2945. doi:10.1364/AO.40.002929

Stramski, D., E. S. Boss, D. J. Bogucki, and K. J. Voss. 2004. The role of seawater constituents in light backscattering in the ocean. Prog. Oceanogr. **61**: 27–56. doi:10.1016/j.pocean.2004.07.001

Stramski, D., and S. B. Woźniak. 2005. On the role of colloidal particles in light scattering in the ocean. Limnol. Oceanogr. **50**: 1581–1591.

Stramski, D., and others. 2008. Relationships between the surface concentration of particulate organic carbon and optical properties in the eastern South Pacific and eastern Atlantic Oceans. Biogeosciences **5**: 171–201.

Twardowski, M. S., H. Claustre, S. Freeman, D. Stramski, and Y. Huot. 2008. Optical backscattering properties of the "clearest" natural waters. Biogeosciences **5**: 495–507.

van de Hulst, H. C. 1957. Light scattering by small particles. John Wiley & Sons.

Van Heukelem, L., and C. S. Thomas. 2001. Computer-assisted high-performance liquid chromatography method development with applications to the isolation and analysis of phytoplankton pigments. J. Chromatogr. A **910**: 31–49. doi:10.1016/S0378-4347(00)00603-4

Wang, J., G. F. Cota, and D. A. Ruble. 2005. Absorption and backscattering in the Beaufort and Chukchi Seas. J. Geophys. Res. **110**: C04014. doi:10.1029/2002JC001653

Woźniak, S. B., and D. Stramski. 2004. Modeling the optical properties of mineral particles suspended in seawater and their influence on ocean reflectance and chlorophyll estimation from remote sensing algorithms. Appl. Opt. **43**: 3489–3503.

Woźniak, S. B., and others. 2010. Optical variability of seawater in relation to particle concentration, composition, and size distribution in the nearshore marine environment at Imperial Beach, California. J. Geophys. Res. **115**: C08027. doi:10.1029/2009JC005554

Zhang, X., and D. J. Gray. 2015. Backscattering by very small particles in coastal waters. J. Geophys. Res. Oceans **120**: 6914–6926. doi:10.1002/2015JC010936

Zheng, G., D. Stramski, and R. A. Reynolds. 2014. Evaluation of the Quasi-Analytical Algorithm for estimating the inherent optical properties of seawater from ocean color: Comparison of Arctic and lower-latitude waters. Remote Sens. Environ. **155**: 194–209. doi:10.1016/j.rse.2014.08.020